Published in final edited form as:

J Opt Soc Am B. 2017 January ; 34(1): 104–129. doi:10.1364/JOSAB.34.000104.

Gas-phase broadband spectroscopy using active sources: progress, status, and applications

Kevin C. Cossel[1,*], **Eleanor M. Waxman**[1,†], **Ian A. Finneran**[2], **Geoffrey A. Blake**[2], **Jun Ye**[3], and **Nathan R. Newbury**[1]

[1]National Institute of Standards and Technology, 325 Broadway, Boulder, Colorado 80305, USA

[2]Division of Chemistry & Chemical Engineering, California Institute of Technology, Pasadena, CA 91125

[3]JILA, National Institute of Standards and Technology and University of Colorado, Department of Physics, University of Colorado, Boulder, CO 80309, USA

Abstract

Broadband spectroscopy is an invaluable tool for measuring multiple gas-phase species simultaneously. In this work we review basic techniques, implementations, and current applications for broadband spectroscopy. We discuss components of broad-band spectroscopy including light sources, absorption cells, and detection methods and then discuss specific combinations of these components in commonly-used techniques. We finish this review by discussing potential future advances in techniques and applications of broad-band spectroscopy.

Molecular spectroscopy has been shown to be a powerful analytical tool with a wide range of applications. The invention of the spectrograph by Fraunhofer in 1814 [1] led to the first broad bandwidth and high-resolution (at the time) studies of the spectra of atoms and molecules [2]. For many years, dispersive spectrometers (and later Fourier Transform spectrometers) continued to be the primary measurement technique due to the lack of high spectral brightness light sources. With the advent of lasers, in particular continuous-wave (cw) lasers, the focus shifted from broad bandwidth to high sensitivity and resolution. More recently, there has been renewed effort to develop systems that can provide the sensitivity and resolution of cw laser-based techniques over a broad spectral bandwidth. Here, we discuss some of the recent developments and hopefully give some insight into future directions the field may take. Because the general field of broadband spectroscopy is so broad, we limit this review to gas-phase transmission spectroscopy techniques using active light sources where sensitivity, bandwidth, spectral resolution, and accuracy are all important. We consider tunable laser sources to be outside the scope of this work.

There are several primary motivations for using broadband spectroscopy as an analytical tool. First and foremost, a large spectral bandwidth allows for the simultaneous detection of

[*]Corresponding author: kevin.cossel@nist.gov. [†]Corresponding author: eleanor.waxman@nist.gov.

OCIS codes. (300.1030) Absorption; (120.6200) Spectrometers and spectroscopic instrumentation; (120.4640) Optical instruments; (300.6390) Spectroscopy, molecular.

multiple species. This enables a single instrument to serve many purposes and also provides a more complete understanding of complex processes. In addition, broad bandwidth enables accurate measurements in complex systems, where interfering absorption from unexpected features can cause significant errors for measurements with a limited spectral bandwidth. However, there are also significant challenges involved with developing sources and detection techniques that can provide the necessary resolution and sensitivity while operating over a wide bandwidth. Figure 1 summarizes the type of broadband source and detection approaches that are considered here. These have been combined in different ways to yield the long list of broadband spectroscopy techniques in Table 1 and discussed in this review.

Because these are all absorption spectroscopy techniques at some level, quantification of trace gases relies on Lambert-Beer's law convolved with the instrument line shape (ILS):

$$I(\nu)=ILS(\nu)\otimes I_0(\nu)e^{-\sum_k \sigma_k(\nu)N_k L}, \quad (1)$$

where ν is an optical frequency, wavelength, or wavenumber, I_0 is the initial intensity, L is the path length, and k are the different absorbers with absorption cross section $\sigma_k(\nu)$ (cm^2/molecule) and number density N_k (molecules/cm^3). For resolved molecular transitions, the cross section can be written as $\sigma(\nu) = \Sigma_n S_n g(\nu - \nu_{0n})$, where the sum is over all n lines, S_n is the linestrength, and $g(\nu - \nu_{0n})$ is the area-normalized lineshape function for a line with center frequency ν_{0n} (see Tennyson *et al.* [3] for recommended lineshape functions). Finally, the number density is often converted to a volume mixing ratio, which gives the mole fraction of the measured species within the sample, and is then expressed typically as part-per-million by volume (ppmv), part-per billion by volume (ppbv), or part-per-trillion by volume (pptv).

The rest of the review is organized as follows. Section 1 provides an introduction to different applications of broadband spectroscopy and their associated requirements. In Section 2, we summarize the different sources, transmission geometries, detection systems used for broadband spectroscopy. Section 3 covers current systems and their applications. Finally, in Section 4 we discuss some of the future directions and applications of broadband spectroscopy.

1. APPLICATIONS

1.A. Atmospheric

Atmospheric measurements are made to monitor air quality and track changes in concentrations of pollutants over timescales of hours to decades. A selection of the important tropospheric species and their corresponding concentration is given in Table 2. Different broad-band techniques are better suited to measuring different classes of trace gases, see Table 2 in [4]. It is often desirable to measure multiple species simultaneously in order to correlate the changes in concentrations of different species to identify sources, such as identifying whether methane emissions are the result of oil and natural gas drilling (in which case it correlates strongly with ethane [5]) or from bovine feed lots (in which case it

often correlates with ammonia [6]). Broadband spectroscopy is an obvious method for this task. In principle, it can provide real-time, *in situ* measurements of multiple gas species. The challenge though is to measure all of the desired species with high enough sensitivity and accuracy in the presence of time-varying absorption from other species (including aerosols), and to make these measurements in the field.

Atmospheric gas sensing can be accomplished by point sensors that use a gas sampling cell or open-path sensors that use a long air path terminated by the detection system or a retroreflector (in principle, back scatter from a surface could be used, but the sensitivity is too low for broadband systems).

Point sensor measurements have been made with IBB-CES and CE-DOAS (Section 3.B) as well as BB-CRDS (Section 3.D). Point sensor techniques are well-suited to mobile platforms (e.g. aircraft) and can be used to measure the source strength of a particular area by driving or flying around the area (e.g. [7–10]).

Open-path measurements average over small-scale turbulent eddies and thus are more representative of the atmospheric composition in an area. In addition, open-path measurements avoid biases due to reactions or losses during sample handling. Historically, open-path measurements have been performed with FTIR (Section 3.A) and with LP-DOAS (Section 3.C); however, these systems have limited path length because of the spatial incoherence of the sources. More recently, quantitative long open-path greenhouse gas measurements have been demonstrated using dual frequency comb spectroscopy (DCS, Section 3.F) over paths of 2 km round trip.

In addition to trace gas detection, isotopic ratios can provide useful data. For example, the CO_2 isotope ratio can track sources of pollution and help identify sources and sinks in the global carbon cycle. Methane isotope ratios can distinguish between anthropogenic and biogenic sources and can provide information about the source of methane in the crust (e.g. microbial vs thermogenic) [11] or in the atmosphere (e.g. fossil fuel vs. biogenic) [12]. Water isotope ratios can track water through the atmosphere, including dehydration methods of water moving from the tropical tropopause to the stratosphere [13] and movement of water through the hydrologic cycle [14, 15]. Comparison of water and CO_2 isotopes between Mars and Earth provides information about gas transfer processes to the Martian atmosphere [16]. Currently, most isotope ratio measurements are performed using mass spectrometry or cw-laser spectroscopy to obtain high sensitivity; however, the ability to measure multiple isotope ratios simultaneously in the field could be a useful application of broadband spectroscopy.

For modeling, it is often not the concentration but rather the flux that is the quantity of interest. The technique of eddy covariance flux measures air-surface exchange of gases [17–21] by correlating the changes in the vertical wind velocity and the concentration of a particular species to determine if the surface is a source or sink of the gas. The measurements need to be at least several Hz in order to capture the small eddies that carry the trace gas in or out of the surface. Because of this requirement, it has only recently been done with broadband spectroscopy when Coburn et al. used a CE-DOAS system (Section

3.B) to measure the fluxes of glyoxal and NO_2 between the ocean and the marine boundary layer [21].

Finally, in addition to the trace gases, the atmosphere includes atmospheric aerosols which are tiny liquid or solid particles suspended in the air. Those with diameters of few microns or smaller are most important for atmospheric chemistry. Sources are both natural (e.g. sea spray produces NaCl aerosols) and anthropogenic (e.g. combustion processes produce soot aerosols). Aerosols both scatter and absorb sunlight with spectra that depend on size and chemical composition. A basic understanding of their scattering and absorption cross sections is needed to accurately model their impact on the climate. Washenfelder et al. used IBB-CES (Section 3.B) to measure the scattering of several different model aerosols including those generated from solutions of ammonium sulfate, fulvic acid, and nygrosin dye [22].

1.B. Chemical Kinetics

Laboratory measurements of kinetics are important to support a variety of fields from atmospheric chemistry [27–29] to combustion [30–34] to fundamental chemistry. These processes are typically complex, with a large number of possible pathways and reactive intermediates that are potentially important drivers of further chemistry. In order to obtain accurate branching ratios for the different paths, the reactants, intermediates, and products all need to be measured. Thus, broadband spectroscopy is an attractive tool if the required bandwidth, sensitivity, and time resolution can be obtained. Example reactions include isoprene chemistry, peroxy radical reactions, ozonolysis of alkenes, and OH radical reactions.

Isoprene is one of the most abundant biogenic VOCs [25]; therefore understanding its reactions and products are important because even species with a small yield from isoprene will be abundant. While the oxidation of isoprene with OH is one of the most well-studied atmospheric reactions (e.g. [35] and references therein), this multi-generation reaction is complex and the chemistry changes with temperature and pollution conditions, leading to unexpected results [36]. Recently, broadband spectroscopy techniques (FTIR and CE-DOAS) were used to measure the first and second generation products from the reaction of isoprene + OH under high NO_x and low NO_x conditions [37].

Organic peroxy radicals (R–O–O$^\bullet$) are important intermediates in atmsopheric and combution reactions and can react with HO_2 to form three different products: organic hydroperoxides (ROOH), alcohols (ROH) and alkoxy radicals (R–O$^\bullet$). The rates and branching ratios for each of these reactions determines the ultimate product distribution for this reaction and these values have been determined using FTIR [38, 39].

The reaction of alkenes with O_3 to form stabilized Criegee intermediates was predicted over 50 years ago, but was finally detected by time-resolved FTS only very recently [40] (see Section 3.A).

In order to observe reactive intermediates, high time resolution (on the order of microseconds) is often required. Two broadband techniques have been demonstrated with

microsecond time resolution: step-scanned FTS (Section 3.A) and time-resolved frequency comb spectroscopy (TRFCS, Section 3.E). The TRFCS system was used to track the photodissociation of deuterated acrylic acid to form *trans*-DOCO with 25 μs time resolution [41] and to measure the *trans*-DOCO radical formed from OD+CO [42].

1.C. Breath Analysis

Human breath contains hundreds to thousands of different compounds in a wide range of concentrations from a few percent for H_2O to parts-per-quadrillion for many volatile organic compounds (VOCs). Some of the most prevalent species are given in Table 3. While many of the molecules in breath are byproducts from daily metabolism, some potentially arise (or change in abundance) due to diseases. The potential use of these molecules as markers for diseases is currently an active area of research, see, e.g. [43–51] for some reviews; however, as highlighted in many of these reviews, there are number of complications such as the lack standardized breath collection procedures and natural variability that cause significant challenges for reliable disease detection. As a result there are currently only a few FDA approved breath tests. Research in medical breath analysis can be divided into two primary directions: detection of a single or a few small species, and detection of many VOCs simultaneously.

All current FDA-approved breath tests rely on small molecules: NO for asthma, CO for neonatal jaundice, and methane for gastrointestinal issues [51, 55]. Other small molecules are current topics of investigation as potential tracers for diseases, including (see also [48]): NO, CO, CO_2, and N_2O [52] or ethane [56] for chronic obstructive pulmonary disease (COPD), acetone for diabetes [57–59], ethane for lung cancer [60], and NH_3 (and possibly methylamines) for kidney function [61, 62]. As in atmospheric chemistry, isotopic ratios can also provide unique information. For example, a change in the abundance of $\delta^{13}CO_2$ can be detected after the ingestion of ^{13}C-labeled substances [51]. Currently, a breath test for gastric infection by *Helicobacter pylori* using ^{13}C-labeled urea is FDA approved with future potential for monitoring liver metabolism [63] and acute liver disease [64].

Unlike for the small molecules, the origin of many of the VOCs in breath is unknown, thus studies tend to look at a large number of VOCs. A number of studies have found tentative correlations between a selected subset of VOCs and diseases [50] such as tuberculosis [65], cancer (see [66, 67] and references therein), and COPD [68]. To date though, no studies have demonstrated robust enough results to provide a clinically useful test.

Despite the potential, breath analysis using broadband spectroscopy has only been preliminarily demonstrated a few times using FTIR (Section 3.A) and near-IR CE-DFCS (Section 3.E). This is at least partially due to the required combination of real-time results, high sensitivity in a low sample volume, and high selectivity against a complex and cluttered spectral background.

1.D. Astrochemistry

The atmospheric composition and chemistry of solar system planets [69] and moons [70, 71] is of interest for understanding planetary formation and can be used to track planetary geophysical processes (e.g., see [72–75]). While it is possible to study these atmospheres

using earth-based telescopes, more precise information can often be obtained with *in situ* measurements [76]. Isotopic measurements of CO_2 and H_2O on Mars [16, 77] show large enrichment of $\delta^{18}O$ for both gases as well as enrichment of $\delta^{13}C$ (which are defined as $\left[\frac{X'/X_{sample}}{X'/X_{reference}}-1\right]\times 1000$, where X' is the tracer isotope (^{13}C or ^{18}O) and X is the standard isotope (^{12}C or ^{16}O) and the reference sample is Peedee belemnite for ^{13}C and Standard Mean Ocean Water for ^{18}O). This, combined with isotope ratio measurements from meteorites, provides evidence for atmospheric loss and ongoing volcanic activity. Active broadband spectroscopy could provide new information on future missions to Mars or other planets, if the system can be made small and compact while maintaining high sensitivity.

Broadband spectroscopy is also important for earth-based observational astronomy. Despite being cold, dilute, and primarily composed of atomic ions, the interstellar medium (ISM) contains a large number of molecules as well, including complex organic molecules [29, 78–81]. Its exact composition is still unknown, as evidenced by a collection of broad bands, collectively called the diffuse interstellar bands [82]. While these have been seen in observational data since the 1920s, only H_2CCC and C_{60}^+ have conclusively been identified as the source of a few of the diffuse interstellar bands [83, 84]. The challenge for laboratory experiments is to replicate conditions in the ISM (i.e. temperature, pressure and concentrations) while maintaining high sensitivity for a wide range of potential molecules. Such laboratory-based studies can both provide reference spectra to support observations and a better understanding of the kinetics of reactions at low temperatures [85–87] to support models of chemical reactions in the ISM. In addition to the ISM, the dense gas and dust that forms stars, and the disks around young stars, are so opaque/cold that only THz and longer wavelength photons can penetrate them. Thus, laboratory THz spectroscopy is necessary to support observations from new observatories such as the Stratospheric Observatory for Infrared Astonomy (SOFIA) and the Atacama Large Millimeter/submillimeter Array (ALMA).

1.E. Industrial applications

In industrial processes, gases must be monitored for purity to avoid contamination for health and/or environmental purposes. Arsine gas (AsH_3) is used in the production of semiconductors. Impurities in the gas at the 10–100 ppbv level can result in lattice structure defects from unintentional doping and currently a combination of different instruments are used to measure all important impurities [88–91]. Reducing this monitoring function to a single broadband system will require a technique with high sensitivity even in the presence of extremely strong absorption from the carrier gas. In a first effort towards this, a CE-DFCS system was developed to measure trace quantities of water in arsine [92].

The combustion of hydrocarbons is an extremely complicated process. Improving the efficiency of combustion systems while simultaneously reducing the emissions of pollutants such as CO, NO_x, and unburned hydrocarbons requires an interplay between laboratory-based kinetics measurements (Section 1.B), modeling, and *in situ* measurements [30–33]. These measurements often must deal with high temperatures and turbulent, fast-flow

conditions while maintaining high sensitivity. A step towards rapid, broadband *in situ* measurements was recently demonstrated using DCS [93].

Broadband spectroscopy also has significant potential for helping industry report emissions of regulated gases and helping regulators monitor and verify the emissions reporting. These emissions include potential health hazards (e.g., VOCs such as benzene, toluene, etc.), clorinated hydrocarbons (CFCs and HCFCs) that deplete stratospheric ozone, and strong greenhouse gases such as CH_4, N_2O, hydrofluorocarbons (HFCs), per fluorocarbons (PFCs, from semiconductor manufacturing), sulfur hexafluoride (SF_6), and nitrogen trifluoride (NF_3). Such measurements have sometimes been performed using FTIR (Section 3.A); however, to measure emissions after abatement systems are in place typically requires higher sensitivity than FTIR can provide.

1.F. Fundamental laboratory spectroscopy

All of these applications – and indeed any other applications of spectroscopy, broadband or otherwise – rely on having accurate line parameters or cross sections that can be scaled to the measurement conditions (e.g., temperature, pressure, other species present) for use in the Beer-Lambert equation (Equation 1). Only with accurate spectral models can complicated spectra be fit to accurately identify weak absorption from a trace species in the presence of strong absorption from other species (e.g., water in the atmosphere or in breath, trace contaminants in high-purity gases). For these measurements, the instrument lineshape (ILS) causes additional complications for determining the cross section or line parameters and thus needs to be known precisely.

Spectral databases such as those listed in Table 4 exist and contain a truly vast collection of spectral information. The gas-phase spectral information has been provided over decades of careful measurements typically with FTIR or grating spectrometers using an incoherent light source. As broadband techniques continue to develop and improve in resolution, sensitivity, and coverage, there is both a need and an opportunity to continue to improve these databases. For example, most of the databases have been developed for standard atmospheric conditions on Earth (with the notable exception of HITEMP [95]), and thus are not accurate for the temperature conditions encountered in combustion systems and on other planets. Frequency combs in particular might be well suited to providing additional high-resolution data beyond those available from FTS because of the inherent combination of high resolution and absolute frequency accuracy. In particular, systems that resolve individual comb modes can have a spectral accuracy at the kHz level (3×10^{-8} cm^{-1}) with no instrument line shape contribution [103–105].

The THz region is also of interest for fundamental laboratory studies because it contains information about intermolecular interactions such as hydrogen bonding dynamics [106, 107], which is critical for a complete understanding of liquid water and solvation dynamics [108]. One of the primary challenges in studying the THz region so far has been the lack of good sources and detectors, although new broadband sources have recently been developed (see Section 3.G).

2. TECHNIQUES

Given the array of possible sources and detection methods, many broadband techniques exist. No one technique is best in all cases, and there is always a complicated tradeoff between system parameters that include: system complexity, spectral coverage (bandwidth and center frequency), frequency resolution, frequency accuracy, and sensitivity at both short times and long times. Sensitivity is often highlighted, however broadband systems will never attain the sensitivity of a single-frequency cw laser system and indeed the whole point is to achieve sufficient sensitivity but across a wide spectrum at high frequency resolution and/or accuracy. In that sense, quantitative comparisons between system sensitivities operating for different purposes and in different spectral regions should be regarded with caution.

2.A. Spectral bands and Sources

Figure 2 displays the regions of the electromagnetic spectrum of interest to molecular spectroscopy, along with available broadband sources. In general, the molecular absorption signals are stronger and richer in the mid-IR and THz and in the UV to visible, but sources and detectors are best developed in the visible and near-IR.

In addition to spectral coverage, sources differ in their spatial coherence, frequency coherence, spectral flatness, cost, size, relative intensity noise (RIN), and so on. Below we summarize these differences for the three important classes of sources.

2.A.1. Incoherent Broadband Sources: lamps, LEDs, Globars—The most readily available thermal light source is sunlight and many systems for atmospheric measurements use scattered or direct sunlight including DOAS, satellite-based spectrometers (e.g. the Orbiting Carbon Observatory-2 [109] and the Atmospheric Chemistry Experiment-FTS [110]), and ground-based FTS (e.g. the Total Carbon Column Observing Network [111, 112] and mobile FTS instruments, e.g. [113]). These systems have been used extensively; however, for obvious reasons they are limited to daytime operation during clear days and are less flexible in terms of measurement path and configuration. For this review, we limit the discussion to active sources.

Broadband spatially incoherent light sources include Xe-arc lamps, deuterium arc lamps (D-arc lamps), tungsten filament lamps, Globar, discharge lamps, or light-emitting diodes (LED) [24]. These sources have the advantage of simplicity and a broad spectrum, but the disadvantage of limited power per frequency and per spatial mode (i.e., high divergence). Blackbody sources such as globars and arc lamps cover the widest wavelength region but require significant power and often have an unstable spectrum (especially for arc lamps). LEDs can provide higher brightness, require significantly lower power, and have a stable spectrum but have a narrower spectrum and are only available in select wavelength regions (mostly in the visible to near-IR).

2.A.2. Supercontinuum—Supercontinuum sources are typically based on a high-power nanosecond- or picosecond-pulsed laser (e.g. Ti:sapphire or Er- or Yb-based lasers), which is amplified and injected into nonlinear optical fiber to create a supercontinuum of light [114–117]. There are a number of different supercontinuum sources (several of which are

commercially available) in the visible and near infrared, which are summarized in Ref. [115, 118, 119], and recent work extends them to the UV and across the mid-infrared [115, 120–124]. Supercontinuum sources have a spectral brightness far in excess of the non-laser-based sources and, moreover, have a spatially coherent output that can support long interaction paths in a cavity or open-path configuration. However, it has been known for a while that they can be substantially noisier than an incoherent source due to technical noise amplification and fundamental limitations from the nonlinear broadening (see, e.g., [116, 125–129]). In particular, the spectrum can vary in shape so that the noise within a narrow spectral bin far exceeds the noise integrated across the spectrum. While the noise does depend on fiber and laser parameters, typically values are ~0.1% to 2% noise in a one second time window for a 0.1 nm bin, see, e.g. [130, 131], with significantly larger shot-to-shot fluctuations [132, 133]. In comparison, a thermal source will have a RIN ~1/bandwidth [134, 135], which corresponds to $<0.01\%$ in a 0.1 nm bin in one second for many thermal sources. Neverthless, supercontinuum sources are an important new tool and have been used in a number of broadband spectrometers discussed later [130, 136–139].

2.A.3. Frequency comb—A frequency comb can be loosely defined as a laser source that produces a spectrum of equally-spaced, phase-coherent lines (or “teeth”) at well-defined and controllable frequencies (see e.g. [140]). Most frequency combs are generated from mode-locked lasers, which emit a series of ultrashort ($\lessapprox$1 ps) pulses at a well-defined repetition rate (typically 100 MHz to 10 GHz). The repetition rate sets the spacing between the teeth in the frequency domain. New, less traditional comb sources that do not necessarily produce pulses (for example, mode-locked quantum cascade lasers, modulator-based combs, and microresonators) are being developed, see Section 4.B for a summary.

The ultrashort pulses from a mode-locked laser result in high peak power, which enables efficient nonlinear effects for spectral broadening or shifting to the UV or the mid-IR using an optical parametric oscillator (OPO) [141–144] or difference-frequency generation [145, 146]. (See [147] for an overview of comb sources for spectroscopy.) The mode-locking process reduces pulse-to-pulse amplitude fluctuations, which typically results in lower RIN even after spectral broadening than a supercontinuum source. However, the spectrum is often significantly more structured with 10 dB or more variation common. Even after spectral broadening, frequency comb sources are also still typically less broad than supercontinuum sources. The advantage of frequency combs though is the lower noise and the increased spectral resolution and accuracy from the comb structure. In addition, the comb structure enables efficient cavity coupling for increased path length (Section 3.E).

2.B. Absorption cells

There are four different types of gas cells shown in the center of Figure 1: a single-pass cell, multipass cell, a resonant cavity, and an open-path system. A single-pass cell is clearly the simplest, might have an effective length of 10 cm to 1 meter and has a spectral bandwidth limited only by the cell windows. A multipass cell uses aligned concave mirrors with an effective path length of 1 m to 400 m [155–157]. The spectral bandwidth and transmission is limited by the multiple mirror bounces. It is relatively easy to couple in to and out of these

cells. In addition, they are relatively insensitive to mechanical vibrations, which makes them attractive for field systems.

A resonant cavity can provide 10 km or more of effective path length but requires well-aligned, high-reflectivity mirrors. The effective path length $L(\lambda)$ is set by the optical losses within the cavity (mirror transmission, scattering, absorption) and is parameterized by the finesse, $\mathcal{F}(\lambda) = \pi/(\text{losses}(\lambda))$: $L(\lambda)$ varies between $\mathcal{F}(\lambda)/\pi$ to $2\mathcal{F}(\lambda)/\pi$ depending on the configuration [158, 159]. Spectroscopy systems use either the fundamental spatial mode, particularly if used with a spatially coherent source, or multiple spatial modes of the cavity, particularly if used with a spatially incoherent source. The challenge for broadband spectroscopy lies in the tradeoff between spectral bandwidth and mirror reflectivity (or path length); typically high finesse can only be maintained for ~10% of the center wavelength. This tradeoff becomes more challenging as one moves from the visible/near infrared into the mid infrared and UV, where the quality of mirrors degrades, which also results in lower throughput for a given mirror reflectivity.

Open-path systems replace the cell with a long open-air sample, often with a reflector so that the light returns to the source where the spectrometer is also located. These systems typically have absorption paths ranging from several hundred meters to 10+ kilometers. The introduction of a long open path is complicated by the presences of atmospheric turbulence, which will both reduce the return power through beam pointing effects and add noise through scintillation. This scintillation is a concern for any scanning system, unless the scan speed is significantly faster than the time scale of scintillation (typically on the order of 10–100 ms, see e.g. [160]), and can result in RIN in the spectrum.

2.C. Detection approaches

In general, the detection systems for broadband spectroscopy can be divided into two broad categories: time-domain acquisition as in Fourier transform spectroscopy, dual-comb spectroscopy, or THz-time domain spectroscopy, and frequency-domain systems as in grating spectrometers or more complicated spectrographs. Each of these systems provide different combinations of wavelength coverage, spectral resolution, number of resolved spectral elements, and time resolution.

The technique of Fourier transform spectroscopy is extremely well developed and discussed in detail in several textbooks [161, 162]. Essentially, one measures the time-domain response of the gas; a Fourier transform then provides the spectrum. Such systems can operate with a single photodetector, which makes them very versatile in terms of spectral coverage. The resolution for a scanning system is typically 0.01–1 cm^{-1}(0.3–30 GHz), with the highest resolution laboratory systems around 0.0003 cm^{-1}(10 MHz). The number of spectral elements is flexible and can be up to 100,000 or more.

The spectrograph category ranges from a low-resolution grating spectrometer to a high-resolution two-dimensional spectrometer that combines a high-dispersion element such as a virtually-imaged phase array (VIPA) etalon [163] (or an Echelle grating [164]) to achieve superior resolution as illustrated in Figure 1. A low resolution spectrometer might have a resolution of ~1 – 10 cm^{-1}(or 0.025 – 2.5 nm at 500 nm) in the visible and near infrared,

while a high-resolution spectrometer can reach 0.03 cm^{-1} resolution. In either case, the dispersed output of the spectrometer is directed to a focal plane array for simultaneous detection of multiple spectral channels (typically 1000–3000, limited by the size of the array). In the visible and near infrared, relatively inexpensive, robust, and high sensitivity Si or InGaAs focal plane arrays are available. Further into the infrared, focal plane arrays are significantly more expensive and have reduced performance.

Regardless of the spectrometer type, if used with a frequency comb source then there is a qualitative difference between situations where multiple comb teeth fall within a single resolution element versus situations where at most one comb tooth falls within a resolution element. In the former, the frequency resolution is set by the spectrometer ILS (instrument line shape) and any frequency accuracy is derived from calibration against known spectra. In the latter, the resolution is set by the narrow comb tooth width (at least for the full width half maximum) and the accuracy is derived directly from the frequency comb. This comb tooth resolution has been achieved for highly coherent dual-comb systems (e.g., [165]), in VIPA-based spectrographs (e.g. [163]), and in Fourier transform spectrometers, particularly if the sampling is synchronous with the comb repetition rate ([166]).

2.D. Sensitivity limits

There are many ways to define the sensitivity of a broadband spectrometer. Research geared towards specific applications will often quote the minimum detectable concentration of the target species which is useful when comparing optical instruments to mass spectrometers. However, this depends on the cross section for that molecule (see Equation 1), which makes comparison between optical systems that measure different species difficult. Instead, in Table 5, we quote the minimum detectable absorbance signal – the quantity $(N\sigma(\nu)L)_{\min}$ – which is the inverse of the mean signal-to-noise ratio (SNR) over a normalized acquisition time (e.g. 1 second).The sensitivity will be wavelength dependent and is often quoted at its peak or averaged over some central portion of the spectrum. It is possible to further normalize by the effective path length to yield an absorbance sensitivity in units of cm^{-1}, which is often done for systems with long interaction lengths through the use of resonant cavity. Finally, in order to compare with swept laser systems, researchers sometimes further normalize by the square root of the number of spectral elements. However, because broadband systems typically cover a much larger spectral range than a swept cw laser, such a comparison is not particularly useful. Indeed, it is important to accept that the spectral SNR of a broadband system will never rival that of a single-frequency system because of spectral brightness limitations. (This reduction is ameliorated to some extent by the fact it is the integrated area of a gas spectrum rather than a peak absorbance that sets its minimum detectable concentration.) Finally, we note that sensitivity is just one feature of any broadband spectrometer and there are always tradeoffs in path length, central wavelength, overall bandwidth, resolution, sensing geometry etc. A system optimized for sensitivity is not as useful, for example, as compared to a fieldable system optimized for the detection of a particularly important trace gas against a cluttered background.

With these caveats, we note there are two types of noise that limit the spectral SNR: (i) white noise that varies randomly across spectral bins as might result from detector noise, shot

noise, broadband laser relative intensity noise (RIN), or digitization noise and (ii) structured or baseline noise that might result from etalon effects, slow variations in the broadband spectrum between normalizations, or other optical and electrical $1/f$ noise. The former will dominate for short averaging times and the latter for long averaging times. Practically, the baseline noise sets the final sensitivity limit. It depends strongly on system design and thus it is difficult to make any general statements.

On the other hand, the random white noise contribution can be analyzed. Discussions of sensitivities for different broadband systems have been presented elsewhere (e.g., Chapter 6 of [161] and [177–179]), so we highlight only a few points here. First, while broadband spectrometers have historically been light limited, as in FTIR or DOAS, that same limit is generally not true with the advent of laser-based broadband sources. In these systems, the maximum signal-to-noise is obtained by increasing the power until detector saturation occurs or relative intensity noise (RIN) becomes the dominant noise source. Both of these cases effectively reflect a “dynamic range” limit. Because of this limit, in non-light-limited situations broadband spectrometers often do not realize the full sensitivity advantage that should be possible due to the higher spectral brightness of laser-based sources (see Figure 2). Instead, researchers can exploit the high spectral brightness by incorporating a much longer effective path length or open path, which is “penalty-free” since the additional insertion loss simply reduces the total power but does not degrade the dynamic-range limited SNR. Second, there is a fundamental difference in the sensitivity between dispersive spectrometers and Fourier transform spectrometers, which arises from the fact that noise is re-distributed across spectral elements after the Fourier transform [161]. Depending on the noise limit, a Fourier spectrometer can result in an improved spectral SNR (if detector-noise limited) or lower SNR (if dynamic-range limited) compared to dispersive detection [161, 180]. However, the gain in wavelength coverage and number of spectral elements from an FTS often outweighs this potential loss.

3. SPECIFIC IMPLEMENTATIONS

3.A. Fourier transform spectroscopy (FTS)

Fourier transform spectroscopy (FTS) using incoherent light sources (including sunlight) was developed in the 1950s [181, 182], see Refs [183, 184] for an interesting history, and soon became the standard infrared spectrometer. In fact, the interest in broadband spectroscopy stems in large part from the remarkable success of FTIR spectrometers, and FTIR data forms the basis for many molecular databases. In addition, FTIRs with incoherent sources have been used to support many of the applications discussed earlier. Commercially available spectrometers can cover up to 5–50,000 $cm^{-1}$by interchanging detectors and light sources (typically incoherent, thermal sources). The resolution varies between 1 cm^{-1} for small, portable systems to ~0.001 cm^{-1} for the highest resolution instruments with 10-m optical delay paths. However, because of the incoherent source, there is a tradeoff between sensitivity, path length, and spectral resolution. In particular, path length enhancement with optical cavities typically results in low sensitivity. Additionally accurate measurements require periodic recalibration [185, 186].

In breath analysis, FTIR was able to detect several VOCs (including hexane, methyl ethyl ketone, toluene, ethanol) in breath [187] at a detection limit of ~1 ppmv using a 4.8-m absorption path. This sensitivity level is suitable for assessing environmental exposure but below the VOCs concentration in normal breath. FTIR was also used to measure $\delta^{13}CO_2$ (using the strong CO_2 band at 4.3 μm) with a precision of ~0.1 ‰(after a correction for temperature drifts) in both atmospheric and breath samples [186] in measurement times of ~2–6 min, although the accuracy (with frequent re-calibration) was not given. In addition, the resolution is not sufficient for many isotopes.

Open path FTIR (see [188, 189] for brief introductions) has been used for several decades in a variety of different applications such as quantification of VOC pollution from manufacturing facilities (e.g., [167, 190, 191]), mapping of NH_3 emissions from agricultural facilities (e.g., [192, 193], measurement of greenhouse gases (e.g., [194, 195]), and quantifying biogenic VOC emissions [196]. These systems typically have 100–1000 m path lengths and achieve an integrated absorption sensitivity of $1–10 \times 10^{-3}$ at a resolution of 0.5–1 cm^{-1} with measurement times on the order of several minutes (limited by the incoherent light sources), longer paths or higher resolution result in reduced sensitivities. This gives detection limits typically in the range of 10s of ppbv for a range of VOCs; however, even with calibration, absolute quantification and agreement between instruments is limited to 10–30% due to uncertainties in the baseline level and the instrument line shape [197, 198].

The time resolution of a continuously-scanning FTS is limited by the time required to scan the optical delay, which is too slow to support chemical kinetic studies. However, higher time resolution can be obtained by using a time-resolved step-scan FTS [199, 200] for repetitive events that can be triggered at a precise time (for example, chemical reactions initiated with laser photolysis). Time-resolved FTS has been used to measure the kinetics of Criegee intermediates, which are formed during the reaction between ozone and alkenes and are thought to be important oxidizers of SO_2 and NO_2 [201–203]. The small Criegee intermediates (CH_2OO and CH_3CH_2OO) formed from the photo-initiated reaction of iodine-substituted hydrocarbons with O_2 were found to have an unexpectedly fast self-reaction rate [204] and conformer-dependent reaction rates in a mixture NO/NO_2 [205]. In addition, the first direct observation of the stabilized Criegee intermediate formed during the ozonolysis of any alkene (in this case β-pinene) was recently accomplished using time-resolved FTS [40].

FTIR systems are commonly used because of the wide wavelength coverage and relative simplicity; however, the sensitivity is not as high as possible due to the the spatially incoherent light source, which limits the path length, and the temporally-multiplexed detection. Given the ubiquity of FTIRs, it is natural to consider replacing the conventional source with either a super-continuum source or frequency comb for increased path length, added sensitivity, or added speed. There have indeed been a number of systems that have done this, e.g., [137, 206–209]; however, some disadvantages of coupling a coherent source with FTIR are that coherent sources are not truly as broad-band as, e.g., a globar and that detection electronics need to be modified to use the additional light available from these sources. In addition, the high RIN of supercontinuum sources can result in lower sensitivity

[137]. The sensitivity limitations of FTIR systems have led to the continued development of other techniques as discussed below.

3.B. Incoherent Broad-Band Cavity-Enhanced Spectroscopy (IBB-CES) and Cavity-Enhanced Differential Optical Absorption Spectroscopy (CE-DOAS)

Incoherent Broad-Band Cavity-Enhanced Spectroscopy (IBB-CES) and Cavity-Enhanced Differential Optical Absorption Spectroscopy (CE-DOAS) are two physically identical measurement techniques based on coupling incoherent broad-band light sources to high finesse cavities. IBB-CES is also called Incoherent Broad-Band Cavity-Enhanced Absorption Spectroscopy (IBB-CEAS) or Broad-Band Cavity-Enhanced Absorption Spectroscopy (BB-CEAS). However, these measurements are actually extinction measurements rather than absorption, i.e. include Rayleigh scattering so we favor IBB-CES. In addition, we prefer to leave “incoherent” in the name to differentiate these LED-based instruments from the cavity-enhanced laser-based instruments discussed later.

These techniques are most often used in the visible and the near-UV, where there exist good detectors and mirrors and strong molecular cross sections, though some systems have recently been built in the near-IR. Initially an Xe-arc lamp was used for the light source [210]. Supercontinuum light sources have also been used more recently e.g. [130, 138]. However, LEDs are most often used since their power requirements are quite low. LED-based instruments tend to be small –with cavities of < 1 meter in physical length – simple, and portable. Typically spectra are recorded on temperature-controlled grating spectrometers. Wavelength calibration is provided by measuring a solar spectrum and instrument line shapes are often determined by measuring lines from e.g. a Hg-line lamp. The instruments do generally require gas cylinders for measuring the mirror reflectivity, calculating the path length, and recording the reference spectrum. They have successfully been deployed on ships and aircraft [21, 211].

These systems, particularly those using LEDs as light sources, are light-limited and photon shot noise or detector noise set the noise limits. This typically limits them to at best minute time resolution. Despite the low photon level, the sensitivity can be excellent because the high finesse of these cavities translates to very long path lengths, often in the range of several to tens of kilometers. For example, the system by Thalman et al. [171] has a path length of up to 18 kilometers. These long path lengths translate to very sensitive detection limits, down to single-digit parts per trillion by volume (depending on molecular cross section strength). Accurate concentration retrievals require careful calibration of the wavelength-dependent path length [171, 212]. Finally, while these systems have several orders of magnitude of linearity, the signal can saturate at concentrations of tens of parts per billion by volume (depending on cross section strength and path length) so they are most commonly used for measuring trace gases with very low mixing ratios.

Figure 3 shows a typical instrument that was designed to measure glyoxal (CHOCHO), methylglyoxal (CH_3COCHO), nitrogen dioxide (NO_2) and the collision-induced oxygen dimer (O_4) in the blue spectral region [171]. The broad-band light source was a blue LED centered at 465 nm that is collimated with a 2” f/1 lens, and filtered with a 420-nm long-pass filter (to prevent UV light from entering the cavity and photolyzing trace gases or initiating

reactions). A portion of the light is coupled into a 100-cm resonant cavity. The light exiting is the cavity is filtered with a band pass filter to remove the green light in the tails of the LED spectrum and focused into a f/4 single-core glass optical fiber and analyzed with a Czerny-Turner grating spectrometer.

The distinction between IBB-CES and CE-DOAS lies in the data analysis. They are both based on Beer-Lambert's law (Eq. (1)). In IBB-CES, the entire broadband spectrum is analyzed after correcting for the mirror reflectivity and Rayleigh scattering [212] and measuring I_0 using purified atmospheric air. In contrast, DOAS retrievals remove the broadband part of the spectrum through a polynomial baseline fit and fit only the narrow band absorbers, thereby relaxing the need for a reference spectrum but limiting detection to molecules that have absorption cross sections that vary rapidly with wavelength. These different processing methods highlight an important issue in any broadband spectrometer, namely the flatness of the spectral response over broad frequency bands and the stability of the light source. This also results in slightly different data acquisition methods: reference spectra are taken significantly more frequently for data that will be analyzed via IBB-CES and significantly less frequently for data that will be analyzed via DOAS.

These systems have found many applications in atmospheric monitoring, both in the lab and in the field. LED-based systems have been used in the UV to measure aerosol extinction [22] and O_3 [213]. They have been used in the blue to measure O_4, NO_2, IO, glyoxal, methylglyoxal, H_2O [171, 214–217] and in the green spectral region to measure NO_3, NO_2, and I_2 [218]. Xe-arc lamps have also be used in the green to measure I_2, IO, and OIO [219]. LEDs have been used in the red spectral region to measure O_2, H_2O, NO_2, NO_3, NO_3 + N_2O_5 [215, 218, 220, 221]. Supercontinuum light sources have also been used in the red [130] and near-IR to to measure CO_2, H_2O, and C_2H_2 [138, 139]. Very recently, a diode laser-pumped Xe plasma was used for measurements from 315–350 nm, below the range of LEDs [222].

3.C. Long-path Differential Optical Absorption Spectroscopy (LP-DOAS)

In LP-DOAS, the cell is replaced by a 100-m to 5-km open air path terminated by a retroreflector array [24, 223]. Xe-arc lamps are needed to supply sufficient spectral brightness, but then limit measurements to fixed locations with sufficient electrical power. The DOAS processing reduces sensitivity to the exact I_0 spectrum, which is measured directly at the light source. This DOAS technique measures species with strong differential cross sections, essentially small molecules in the UV and visible, including HONO, NO_2, HCHO, O_3, and NO_3. Unlike the cavity-based system, LP-DOAS is also free of wall losses and sampling line losses, providing a true path-averaged in situ measurement. These instruments also tend to be light-limited so photon statistics determine the detection limit although other systematics (such as residual structure) also play a role. Typical systems can achieve a minimum detectable optical density of 5×10^{-4} in ~5 min [24], which gives detection limits in the few to hundreds of parts per trillion by volume for trace gases, including 160 pptv for NO_2, 830 pptv for formaldehyde, and 78 pptv for HONO.

LP-DOAS has been used for atmospheric measurements for decades (e.g. [224–226]). It was used to measure O_3, NO_2, SO_2, HCHO, HONO, BrO, ClO, and IO in the marine boundary

layer in Mace Head, Ireland [227]. During a large campaign in Mexico City in the spring of 2003 LP-DOAS measured glyoxal, HCHO, NO_2, and O_3 across a 4.42 km path in the blue and UV spectral regions [169]. Another LP-DOAS instrument measured formaldehyde and a number of aromatics during the same campaign [228]. This technique was also used to measure vertical profiles of NO_2, NO_3, O_3, HONO, and HCHO in Phoenix, Arizona [229] and to obtain vertical profiles of O_3, SO_2, NO_2, HCHO, and HONO over Pasadena, California during CalNex 2010 [230]. Detection limits for this technique range from 3.2 pptv for NO_3 to 2.3 ppbv for O_3 (measurement time not specified) [230].

3.D. Broad-Band Cavity Ringdown Spectroscopy (BB-CRDS)

Cavity ringdown spectroscopy (CRDS) uses a laser source coupled into a high finesse cavity. The laser is turned on for a period of time to let light build up in the cavity, and then turned off at which point an exponential decay of the light is detected. The decay rate is compared in the presence and absence of an absorber, which allows the concentration of the absorber to be calculated [231, 232]. The advantage of this ring-down approach is that is insensitive to amplitude noise of the source. However because traditional CRDS is done at a single wavelength, it is subject to interferences by other species that absorb at the same wavelength and cannot be used to retrieve multiple species simultaneously.

Broad-band CRDS can circumvent this limitation. BB-CRDS has been achieved in a number of ways by coupling lasers to high-finesse cavities, see the comprehensive review of early techniques in [168]. The first demonstration measured the O_2 A band. They used a pumped dye laser with a 400 cm^{-1} spectral bandwidth, coupled to a cavity with an effective path length of 560 meters. Light exiting the cavity was coupled to a FTS followed by a photomultiplier tube, which allowed the users to collect ring-down spectra for individual wavelengths by setting the mirror position on the FTS [233]. A second demonstration presented a technique called ringdown spectral photography (RSP) to measure propane. This also used a Nd:YAG-pumped dye laser that was then directed onto a mirror that rotates, scanning the light across a diffraction grating which then directs the diffracted light onto a 2-D CCD camera using streak detection [234]. This was the first implementation to achieve simultaneous time and wavelength resolution, as the work in [233] measured single wavelengths at a time from a broad-band source. Another demonstration used a Nd:YAG-pumped dye laser coupled to an imaging spectrometer plus a clocked 2-D CCD camera to measure NO_3 and H_2O [168, 235]. Yet another demonstration coupled a frequency comb to a cavity and aligned the comb pulses with the cavity modes. This used a detection system very similar to the RSP system [236].

3.E. Cavity-Enhanced Direct Frequency Comb Spectroscopy (CE-DFCS)

In cavity-enhanced direct frequency comb spectroscopy (CE-DFCS) or mode-locked cavity enhanced absorption spectroscopy (ML-CEAS), a frequency comb is coupled into a high-finesse cavity, as discussed in several recent reviews [147, 158, 209]. The advantage of using frequency combs is that the cavity mode spacing and comb mode spacing can be matched, so a significant fraction of the comb light is coupled into and out of the cavity. However, due to dispersion in the enhancement cavity, this matching is only possible over some limited bandwidth. Moreover, it is technically challenging. There are two primary ways of ensuring

this matching of comb and cavity modes: the first is a swept lock where the comb teeth and cavity modes are periodically swept into resonance with each other [158, 237], while the second is to maintain a tight lock between the comb teeth and the cavity modes, typically using a Pound-Drever-Hall locking scheme [172]. In the latter, frequency noise can be mapped to amplitude noise, thus reducing the sensitivity unless this noise is suppressed, e.g. [175, 179]. The swept approach removes this problem by rapidly integrating over the cavity transmission peak, avoids the cavity-dispersion limitation to the spectral bandwidth, and avoids the problem of lineshape distortion [172]. However, the swept approach reduces the transmitted light and adds a temporal variation to the transmitted intensity, which can be problematic for some detection methods.

The cavity-transmitted light must then be spectrally detected. Several different detection systems have been used for CE-DFCS: dispersive spectrographs using a grating spectrometer (e.g., [173, 237]) or a VIPA spectrometer (e.g., [41, 92, 170]), scanning Fourier-transform spectrometer (e.g., [172, 179, 238]), and dual comb spectroscopy ([239, 240]). Each measurement system has its own set of compromises for spectral coverage, resolution, measurement speed, and noise performance (i.e., suppression of amplitude noise from the cavity-comb coupling). A summary of some demonstrated CE-DFCS systems illustrating these tradeoffs is given in Table 5.

In support of breath analysis, Thorpe *et al.* performed an initial demonstration of the measurement of NH_3, CO, and CO_2, as well as isotope ratio measurements for CO_2 in breath using near-IR CE-DFCS [170]. They obtained an absorbance sensitivity of 2×10^{-3} in a 30 s measurement time using a 1.5-m-long cavity with an effective path length of 27 km. This provides a detection limit of 900 ppbv for CO and a projected sensitivity for NH_3 (determined by measuring NH_3 in N_2 and comparing with the breath spectrum) of 18 ppbv. Because of the low linestrengths in the near-IR, these detection limits could be improved by moving to other wavelength regions.

CE-DFCS has been applied to atmospheric measurements in the field. In Ref. [241, 242] IO, BrO, and NO_2 were measured for several months at a coastal East Antarctic site. In this system, the frequency comb source was coupled into two ~90-cm long cavities with a finesse of 6,000 at 338 nm or 32,000 at 436 nm using the swept lock and detected with a 0.45 cm^{-1}(5 pm) resolution spectrometer. The system achieved a minimum detectable absorbance of $\sim 9 \times 10^{-5}$ in 1 min, which is an order of magnitude lower than the comparable LED-CE-DOAS system [217] and two orders of magnitude lower than comparable IBB-CES systems [212, 214]. The tradeoff here is increased weight, power consumption, and complexity. The measured 1σ detection limits were 1 pptv for BrO, 100 pptv for H_2CO, 40 ppqv for IO, and 10 pptv for NO_2 with 1 min acquisition time.

CE-DFCS has also recently be adapted to measure rapid chemical kinetics in a technique called time-resolved frequency comb spectroscopy (TRFCS), as shown in Figure 4. In the first demonstration of this technique [41], the production of the *trans*-DOCO radical from the photodissociation of deuterated acrylic acid was measured with a time resolution of 25 μs. This system is based on a mid-IR frequency comb source plus a VIPA spectrometer for frequency resolution and obtains high time resolution by gating the integration time of the

camera. The simultaneous bandwidth is limited by the spectrometer to 65 cm^{-1} and is tunable over a wide range. The broad spectral bandwidth enabled the measurement of the precursor (i.e., deuterated acrylic acid) depletion, reactive radical (*trans*-DOCO), and final products (HDO and D_2O). In addition, a completely unexpected species, deuterated acetylene, was observed as a prompt photodissociation product. This suggests that even this fairly simple photodissocation process is not well understood and illustrates the advantage of broad bandwidth for kinetics measurements. Subsequent measurements applied this system to studies of the OD+CO reaction, which is important in both atmospheric chemistry and combustion dynamics, and provided the first direct measurement of the *trans*-DOCO radical formed during this reaction [42].

3.F. Dual comb spectroscopy (DCS)

The basic concept of a coherent dual comb spectrometer is illustrated in Figure 5 and is reviewed in [178]. This technique relies on the interference between two combs with slightly different repetition rates. In the frequency-domain picture, the two combs have slightly different tooth spacings so that their heterodyne beat signal leads to a comb in the rf domain, thus mapping the optical information to easy-to-measure rf signals. In the time-domain picture, the two comb sources produce pulse trains with different periods. As the pulses from one comb “walk through” the pulses of the second comb, the pulse-by-pulse overlap is digitized. This results in a scanning much like the interferometer used in FTS, but with the scanning done optically. The resulting interferogram is a down-sampled measurement of the source pulse after transmission through the gas; any gas absorption signature appears as a trailing free-induction decay. For high SNR, the dual comb spectrometer requires high coherence between the combs [177, 243], which can be accomplished with optical locking or signal processing. Most DCS systems are currently limited to the near-IR, where robust comb sources exist, but there is ongoing work to develop systems in the mid-IR to access the larger molecular cross sections [178].

The time required to acquire a single interferogram is given by the difference in the comb repetition rates, $1/\delta f_{\mathrm{rep}}$, and can be on the order of milliseconds. However the Nyquist sampling criterion limits this interferogram acquisition rate to $\delta f_{\mathrm{rep}} < \frac{f_{\mathrm{rep}}^2}{2\delta\nu}$, where f_{rep} is the comb repetition rate and $\delta\nu$ is the spectral bandwidth. Only then is there the desired one-to-one correspondence between the rf comb teeth and pairs of optical comb teeth. In other words, the broader the spectrum or lower the comb repetition rate difference, the longer the interferogram takes. Higher time resolution can be obtained with apodization, but this results in lower spectral resolution and prevents mode-resolved measurements.

DCS is potentially well-suited to atmospheric measurements since the high frequency resolution makes it possible to measure multiple species simultaneously in a complex background. Additionally, the coherent and collimated laser light allows significantly lower optical powers of light to be used in comparison to long-path DOAS (see Section 3.C). The rapid acquisition rate also eliminates potential spectral distortions due to atmospheric turbulence. However, the added complexity of the system has resulted in a limited number of demonstrations of open-path DCS. The first demonstration was used to temporally resolve NH_3 plumes from an open gas cylinder outside of a lab [244] across a 44-m-long path. This

experiment used two mid-IR combs created from difference-frequency generation of 125-MHZ Ti:sapphire lasers focused in to Ga:Se crystals. This produced 10 μW of mid-IR light covering 840–1120 cm^{-1}(8.9 to 11.9 μm). Spectra were measured at 2 cm^{-1} resolution with a 70 μs update rate; however, the sensitivity and accuracy were limited due to the unstabilized combs.

The first quantitative demonstration of open-path DCS was used to measure the greenhouse gases CO_2, CH_4, H_2O, and HDO over a 2-km round-trip path [176] using laboratory-based combs. This work was done in the near-IR (6000 to 6250 cm^{-1}or 1.60 to 1.67 μm) using overtone bands of the gases. Two erbium fiber-frequency combs with 100 MHz repetition rates were used as the light source. They were combined and launched off a telescope to a 50-cm diameter plane mirror located 1 km away from the light source. The light was reflected back to the source, collected in a fiber, and sent to a detector. This system was also used to measure spectral phase by launching only a single comb (see Figure 5 and [245]). An open-path measurement over ~26 meters round-trip was also done with a single comb (rather than a dual comb setup) in the mid-IR to measure CH_4 and H_2O [246]. They used a pumped OPO to created the comb spectrum, sent the light over 13 meters to a retroreflector, and collected the light with a telescope before sending it to a VIPA and camera for detection.

Dual frequency comb spectroscopy with coherent, stabilized combs is also a new tool for generating precise spectra in support of improved molecular databases because of the negligible instrument line shape. Zolot *et al.* [104] demonstrated broadband, high accuracy measurements of C_2H_2 and CH_4 using dual frequency comb spectroscopy cover 5800–6700 cm^{-1}(1.5–1.7 μm). They determined a systematic uncertainty on the line centers of 0.2 MHz (7×10^{-6} cm^{-1}) and an SNR-limited precision of $\sim 10^{-4}$ of the line width on the strongest lines. DCS has also be used to simultaneously cover 5260–10000 cm^{-1}(1.9–1.0 μm) [105] while still maintaining high precision and accuracy, allowing retrieval of line centers of C_2H_2, CH_4, and H_2O. Baumann *et al.* [103] have demonstrated a line center accuracy of 0.3 MHz for CH_4 using DCS in the mid-infrared, which is an order of magnitude below the accuracy of FTIR measurements. DCS can also provide new information about line broadening parameters; for example, Iwakuni *et al.* [247] recently measured nuclear-spin-dependent pressure broadening in acetylene in the near-IR.

3.G. THz Time-Domain Spectroscopy (THz TDS)

The most widely used broadband THz spectroscopy is likely THz time domain spectroscopy (THz-TDS). In THz-TDS, one measures the electric field of a THz pulse in the time domain after transmisison through a sample. This enables the direct determination of the broadband optical constants of a material [248]. Additionally, THz-TDS can be used in studies of ultrafast dynamics, as the THz pulses are single-cycle and near transform limited in the time domain [249]. The spectral coverage, given by the Fourier transform of the THz pulses, can be very broad, often covering 10 THz or more for a particular source/detector combination, with a high peak dynamic range (>60 dB) [248]. Another common feature of THz-TDS pulses is their fixed carrier envelope phase (CEP) offset, which is a requirement for repetitive time domain electric field sampling. The resolution of THz-TDS instruments is typically ~1 GHz (limited by the length of mechanical delay lines), but the fixed CEP of

oscillator-based systems can be exploited for resolutions of <10 kHz, particularly in asynchronous optical sampling (ASOPS) designs [154, 250, 251].

A typical THz-TDS setup is shown in Figure 6, and consists of an ultrafast laser (often Ti:Sapphire or fiber based), THz emitter, optical delay line, and THz detector. Here, we discuss several emitter/detector methods that have been used for THz-TDS, and emphasize the inherent trade-offs of each. Most emitter techniques can also be used for detection, but the emitter and detector need not be based on the same proceess. For example, a plasma emitter can be used with a nonlinear crystal detector, or vice versa.

The earliest THz-TDS designs used a photoconductive antenna (PCA) switch as both emitter and detector [252]. This method is still used in oscillator-based systems for moderate bandwidths of several THz [251], and can be extended to 20 THz of generation bandwidth with sufficiently short optical pulses [253]. The active area is often improved with an interdigitating arrangement [254].

Nonlinear crystals comprise the second major class of THz-TDS emitters and detectors. Inorganic crystals with a large second-order (nonlinear) susceptibility, such as ZnTe, GaP, $LiNbO_3$, GaAs and GaSe, are most commonly used for THz generation via optical rectification and difference frequency generation [255–260]. Organic crystals, such as DSTMS, DAST, and OH1, have also been used due to their exceptionally large nonlinear coefficients [261]. Phase-matching between the optical or near-infrared pump light and THz light as well as crystal phonon absorptions can limit the bandwidth and conversion efficiency attainable with a particular nonlinear crystal. This leads to an inherent tradeoff between bandwidth and conversion efficiency for different nonlinear crystals in various sections of the THz. Nevertheless, THz generation from nonlinear crystals pumped by amplified ultrafast laser systems have yielded some of the largest THz pulse energies (~270 μJ) [261] and focused field strengths (50 MV/cm) [262] of any THz technique, enabling the first demonstrations of broadband multidimensional THz spectroscopies of gases [263], liquids [264, 265]. and solids [266].

The third, and most broadband, class of THz-TDS techniques is two-color plasma filamentation [267, 268] and the related air-based coherent detection [269, 270]. The main difficulty of these techniques is their reliance on ultrafast amplified laser systems with mJ level pulse energies. For generation, a focused, high intensity pulse with frequency ω ionizes the molecules or atoms in a gas, creating a plasma. By spatially and temporally overlapping a second ultrafast pulse of frequency 2ω on the plasma, broadband THz radiation is generated that can span >100 THz of bandwidth [271]. For plasma detection, an intense gating pulse of frequency ω is focused to generate a second gas plasma and overlapped with the THz radiation between a pair of biased electrodes [269]. The mechanisms of THz generation are still under active investigation, but involve a combination of four-wave mixing, asymmetric photo-induced currents, and current oscillations [272]. The broadband pulses from two-color plasma filamentation are attractive for linear spectroscopic applications, as they provide continuous coverage from the microwave to the mid-infrared regions of the spectrum. Their subcycle temporal profile and relatively intense pulse energy are also ideal for studies of the coherent control of materials.

As in other spectral regions, broadband THz sources can also form frequency combs, either by downconversion of a modelocked near-infrared oscillator (often in a THz-TDS setup) [154, 250, 251, 273], directly from a THz quantum cascade laser [274–276] or from coherent synchrotron radiation [277]. Downconversion to a THz comb is typically accomplished with a photoconductive antenna (PCA) or a nonlinear crystal. A PCA emitter driven by an 800 nm 80 MHz oscillator can generate a THz comb spanning 2.5 THz with ~10 μW total power spread over ~30,000 comb teeth (~300 pW/tooth). Broadband detection of a THz comb has been demonstrated with ASOPS THz-TDS [154, 250, 251, 273], and is directly analogous to dual comb techniques used at higher frequency (see Section 3.F).

THz combs can also be generated from coherent synchrotron radiation (CSR), which can provide total powers of 60 μW over bandwidths of ~1 THz. In an initial demonstration, a comb tooth spacing of only 846 kHz was reported (20 pW/tooth), due to the long revolution period of the electron bunches in the synchrotron storage ring [277]. This spacing is well-suited for molecular spectroscopy, as it is near the Doppler linewidth of small molecules in the THz range. However, unlike other approaches, a CSR source requires a dedicated user facility.

Finally, new laser sources have recently been developed in the THz region. In particular, quantum cascade lasers (QCLs) can directly emit in the THz region with milliwatt output powers and octave spanning bandwidths [278]. QCLs can also be quite compact, which could lead to monolithic THz comb sources. Modelocked THz QCLs should form a comb, have so far been limited to narrow bandwidths (0.1 THz) [279]. QCL combs generated from four-wave mixing can generate larger bandwidths (0.6 THz), with integrated dispersion compensation [274, 276]. In these designs, 70–80 teeth can be produced with milliwatt power levels, or individual tooth powers of ~50 μW. They are only suitable for frequency domain applications, however, as they do not form time-domain pulses [274].

The absorbance sensitivity at 1 s of averaging of THz TDS instruments is $\sim 5.0 \times 10^{-1}$ for 1 GHz frequency resolution [280]. Dual THz comb systems achieve much higher frequency resolution with lower sensitivities [154, 251]. This is due to the longer delay times needed to resolve individual comb teeth. Overall, the sensitivity of oscillator-based THz-TDS systems is limited by detector noise.

Compared with broadband spectroscopy in the near-and mid-infrared, THz-TDS is still in its infancy. Initial demonstrations in trace gas sensing, however, highlight some possible future applications of THz-TDS [280–282]. For example, in 2016 Hsieh *et al.* used ASOPS THz-TDS to measure acetonitrile gas at atmospheric pressure in the presence of smoke from a burned incense stick [280]. Scattering losses from smoke particulates make this a challenging measurement at higher frequencies, but Hsieh et al. reported no measured loss in the longer wavelength THz transmission. At 1 s of integration the detection limit of acetonitrile was 200 ppmv, while they also estimated higher detection limits of HCN (200 ppmv) and SO_2 (700 ppmv). While these detection limits are higher than in the near- or mid-infrared, the recent development of plasmonic photoconductive emitters should improve measurement sensitivities by 10–100× [283]. The transmission of THz light through samples opaque in the infrared and visible is also attractive for sensing of concealed explosives, and

THz-TDS has been demonstrated as an effective tool for differentiating explosives based on their characteristic vibrational and phonon absorptions [284]. A related application is the non destructive examination of space shuttle tiles with THz-TDS, particularly in corrosion and defect detection [285].

4. FUTURE DIRECTIONS

With the continued rapid development of new sources and techniques, we envision a parallel rapid expansion of broad-band spectroscopy across the applications discussed in Section 1. In this section, we first emphasize some of the unrealized potential of broadband spectroscopy, which is largely driven by the lack of highly sensitive, fieldable systems. We then discuss important advances in sources, sampling cells, and analysis that might enable a new class of instruments that does have the size, sensitivity, accuracy, and robustness to support real-world applications of broadband spectroscopy.

4.A. Forward-looking implementations of broadband spectroscopy

Medical diagnosis, in particular breath analysis (see Section 1.C), is a potential widespread application but it requires significant additional research. Specifically, further research is needed to identify strong correlations between the concentration of particular trace gases and a disease. This in turn requires robust statistics and thus a very large sample size. To support this level of statistics, as well as any future clinical use, we envision a small and robust instrument that could be located in hospitals or other medical facilities, rather than a large, complex instrument in a research laboratory. Moreover, this sensor will need the speed and sensitivity to detect trace gases in relatively small sample volumes and against a cluttered background.

Atmospheric chemistry (see Section 1.A) is another broad area that could benefit dramatically from improved broadband spectrometers. As with breath analysis, atmospheric field measurements have stringent requirements on size, robustness and sensitivity. In addition, for eddy-covariance or airborne sensors, high speed is also required. The development of small, inexpensive, portable, accurate, sensitive instruments (such as miniature greenhouse gas sensors or other trace gas sensors) will allow new measurement networks to be developed and, if sufficiently low in price, would enable crowd-source measurements. This could enable cities to monitor their emissions in real time with high spatial resolution, which is important for minimizing emissions [286], as well as monitor air quality (e.g. O_3 concentrations) at high spatial resolution in real time, thus limiting the health impacts of poor air quality. This development could also enable sensors to be placed on novel platforms, such as UASs and weather balloons which could allow increased measurement frequency, decreased cost for monitoring, and routine vertical profiling, which would couple nicely with atmospheric satellite measurements. Open-path instruments with extremely long path lengths could enable active satellite-based measurements (e.g., to a detector on the ground), which would allow for night-time measurements and measurements near the poles (both of which are not possible with current passive satellite systems). For long-path measurements in populated areas it is of course critical that care is taken to keep the light sources eye safe while still maintaining high sensitivity.

These advances in sensors are not limited to supporting *in situ* gas measurements. For example, ice cores provide information about the history of the atmosphere and drivers of climate events [287–290]. With more sensitive instruments that require a smaller gas volume, it would be possible to use a cavity-enhanced system to simultaneously measure multiple gases (and isotopic ratios) in ice cores, extending the history of some trace gases back significantly into the past. In addition, improved sensitivity with faster acquisition times and broader bandwidth will enable further measurements of reaction intermediates, perhaps enabling the detection and quantification of key intermediates in atmospheric and combustion reaction cycles. As another important example, organic aerosols are a topic of significant interest in the atmospheric community [25, 291, 292] and sub-micron aerosols are a health concern [293–296]. The chemical composition of aerosols is often measured with aerosol mass spectrometers, which provides invaluable information about the bulk composition of aerosols, but fragments molecules and makes it difficult to unambiguously identify compounds; there is growing interest in identifying what fraction of the organic aerosol mass is due to specific organic compounds [297, 298]. A small, portable, cavity-enhanced instrument could be incorporated into an aerosol mass spectrometer prior to the fragmentation process to identify specific organic molecules present in the aerosol.

Finally, we anticipate that applications of THz spectroscopy will become more prevalent as sources and instruments improve. For example, the ability to measure spectra through clouds, smoke, and haze creates intriguing possibilities for atmospheric field measurements. Laboratory THz spectroscopy could also be useful for studying the chemistry of organic aerosols and the chemistry on ice grains. Further, high-resolution space-borne absolute measurement instruments would be very useful in advancing THz spectroscopy of the ISM and support Earth-based observatories.

Above, we emphasize some of the potential for future medical diagnostics and atmospheric chemistry. However, similar potential exists across all the applications listed in Section 1. Again, we emphasize that detection alone of a trace gas is often not sufficient; in addition, some level of precision and accuracy is needed. The real challenges lie in meeting these sensitivity/precision/accuracy requirements within a sufficiently robust and spectral broadband sensor.

Future widespread adoption of broadband spectroscopy will be driven by technical advances in a number of critical areas including the sources, sampling approaches, and ability to deal with “clutter”, i.e. the fact the measured spectra are extremely complex with contributions from multiple energy levels across multiple gas species. We discuss these potential advances below.

4.B. Advances in broadband sources

There are number of new technologies for reducing the size and complexity of broadband mid-infrared, visible-to-UV, or THz lasers. This includes using robust and compact near-IR fiber lasers plus chip- and/or fiber-based non-linear optics to cover new wavelength regions as well as developing sources that directly emit in these regions.

The wavelength coverage of comb systems based on robust fiber laser technology [152, 299, 300] is being extended using non-linear optical techniques. In particular, difference-frequency generation (DFG) technology is continuously improving and has been used to generate high power (100–500 mW), tunable frequency combs in the mid-IR out to 5 μm[145, 301, 302], out to 14 μm with lower power [303], and with wide spectral coverage [146]. As these systems improve and in particular with the development of flexible, tunable waveguide non-linear devices, they will be able to provide higher power in a more integrated, robust package. An exciting demonstration of this potential was shown by Iwakuni *et al.* [304], where a single fiber comb combined with highly nonlinear fiber and then a waveguide periodically-poled litium niobate crystal generated coherent light spanning from 350 nm to 4.5 μm. Optical parametric oscillator systems have also been developed to extend past 5 μm[142–144]. New chip-based nanophotonic non-linear devices [305] based on silicon [306–308], silicon nitride [309], and other materials are being developed. These devices have advantages over non-linear fiber for continuum generation since they can be smaller, fully integrated, and offer wide dispersion control by tuning the waveguide shape and height [310], which translates into control over the generated spectrum.

Frequency comb generation has also been achieved using nonlinear effects in a high-finesse microresonator pumped with a cw laser (see, e.g., [311–315]) and dual comb spectroscopy using such combs was recently demonstrated [316]. Such microresonator combs are promising for compact sources in the UV/visible through the mid-IR and potentially THz, but several challenges need to be addressed: careful control is required to ensure true comb generation [317–319]; microresonator combs often have high repretition rates (~100 GHz), which is difficult to use for many spectroscopy applications; and, despite the microresonator being small, these typically require off-chip pump lasers with bulky and sensitive coupling setups required to pump the microresonator.

Finally, frequency combs can be generated by use of an electro-optic modulator to apply sidebands to a cw laser [320, 321]. This technique can be compact and robust, especially with new fiber-coupled modulators with very high modulation depth, but have a fairly limited bandwidth and currently only operate in the near-IR. However, such combs have recently been used for dual comb spectroscopy [240, 322, 323]. Another intriguing possibility for spectroscopy is to use an electro-optic modulator to increase the mode density from a microresonator comb [324].

In addition to the use of non-linear optics, new laser sources are being developed to directly access additional spectral regions. In the THz, new emitter materials will significantly increase the available power and spectral coverage (e.g., [261]). In the mid-infrared, quantum cascade lasers (QCLs) and interband cascade lasers, (ICLs) have compact size and broad wavelength flexibility. Frequency comb generation using a QCL was demonstrated a few years ago at 7 μm [325] and has been extended in the mid-infrared and THz (see [153] and references therein and Section 3.G). QCL combs have recently been used for a proof-of-principle demonstration of dual comb spectroscopy using two separate QCLs [326] and two QCL combs on a single chip [327]. Currently, QCL combs are limited to ~ 100 cm^{-1} of bandwidth, with significantly improved bandwidth they could be attractive sources for applications.

4.C. Advances in compact sampling cells

For any point sensor, the sensing cell is a critical component and can drive the overall sensor size and limit the overall sensor performance. Of course, there is always a trade-off between path length and sensitivity, but this can be somewhat compensated for by increasing the cavity finesse and operating in spectral regions with larger absorption cross sections.

Recently, compact multipass cells have been developed that achieve a total path length of 4.1 m in a total volume of only 40 mL [157]. These cells have the potential to operate from the visible to the THz. In another approach, hollow mid-IR waveguides have been fabricated with interaction paths on the order of 10 cm and small sample volumes [328, 329]. Finally, resonant optical cavities can be miniaturized, including mm-scale fiber Fabry-Perot cavities formed between mirrors machined on the tips of optical fibers [330, 331]. These cavities have extremely small mode diameters, thus the integration volume is small. The mode spacing of these cavities is 100 GHz, which is too wide for some spectroscopy applications. However, it may be possible to scan the length and thereby fill in spectral gaps. With continued 5–10x improvements in physical length and mirror reflectivity, such cells could provide long effective paths in extremely compact, integrated cavities with small sample volumes.

The use of resonant cavities does rely on mirror coating technology. The quality of coatings in the UV and the mid-IR is limited by absorption and material scattering losses, which leads to lower finesse than in the near-IR or visible. In addition, standard coatings usually provide a useful bandwidth of ~10% of the center wavelength, so that several different cavities are required to cover a broad spectral range. The bandwidth of a standard cavity is related to the index contrast between the layers in the Bragg stack. Thus, the development of high-index-contrast coating materials would be a worthwhile endeavor. In recent work, a novel optical coating technology for the mid-IR was developed using crystalline mirror technology [332]. These coatings have demonstrated extremely low scatting losses in the near-IR that should extend out to 7.5 μm. Perhaps more exciting though, since these mirror coatings use molecular-beam expitaxial growth (a common process for semiconductor manufacturing) instead of the usual electron-beam or ion-beam sputtering, this approach could also take advantage of new materials with high index contrast [333–335]. Optimistically, one could envision mid-IR cavities with a finesse of a few thousand spanning a full octave or more. Another route to a broad bandwidth cavity is to rely on total internal reflection instead of interference from a multi-layer Bragg reflector. This has been accomplished by use of two right-angle prisms instead of mirrors [336]. For example, a fused-silica prism cavity has been demonstrated with a finesse better than 10,000 from 550–750 nm [136]. The wavelength coverage can be extended to cover the visible to UV using CaF_2 [337] or to reach the mid-IR using BaF_2 [336] or potentially other materials such as KRS-5.

4.D. Advances in broadband spectrometers

In Section 2.C, we outlined the basic approaches used in broadband spectrometers. As the base technology of detectors, focal plane arrays, optical components, and digital signal

processing (e.g. field programmable gate arrays and digital signal processors) improve, we expect continued improvements in the robustness and performance of various designs.

However, we emphasize that all designs face a common critical challenge. The overall goal for broadband spectroscopy systems is to sensitively and accurately determine the amount of absorption, which requires a determination of the baseline (i.e., the zero-absorption level). This requires measurement of I_0 and is significantly more challenging than might be naively assumed; indeed, the capability of measuring the zero-absorption level needs to be designed into systems and rigorously tested. There are two obvious approaches: either a separate reference channel is measured, or, if the absorber concentration can be turned off, the reference spectrum is measured by time multiplexing. Clearly, the separate reference channel must be designed to be as similar as possible to the measurement channel (which is often hard to do with cavity systems or long-path systems). For time-multiplexed approach, the light sources must be stable in power and in spectrum over sufficiently long times. In future systems, one would expect a series of approaches that together reduce the system sensitivity to these “baseline” issues.

4.E. Analysis of complex spectra

Finally, we emphasize that as broadband spectrometers produce ever higher resolution, accuracy and SNR spectra, we require a parallel advance in the acquisition and analysis of complex spectra to exploit these advances.

At a minimum, this requires accurate molecular cross sections and lineshape models, as discussed in Section 1.F. Even for unresolved absorption features, high-resolution, broadband spectroscopy is necessary to accurately measure cross sections as a function of temperature and pressure. Many of these databases are built on older FTIR spectra that might not equal the resolution and accuracy possible with laser-based systems.

However, it is inevitable that broadband spectra will be complex as they cover many thousands of molecular lines. Therefore, the community must develop new techniques to simplify the spectrum or to further multiplex the spectral readout. Cooling the gas sample can drastically reduce the number of molecular absorption lines by reducing the initial number of populated states (from the Boltzmann distribution). In addition, Doppler broadening is significantly reduced, so the lines are much narrower. Mid-IR CE-DFCS was recently combined with buffer-gas cooling (using cold He gas, [338]) that reduced the sample temperature to 10K or below, yielding resolved spectra of fairly large, rigid molecules such as napthalene ($C_{10}H_8$), adamantane ($C_{10}H_{16}$), and hexamethylenetetramine ($C_6N_4H_{12}$) around 3 μm[339]. Intramolecular vibrational redistribution limits the type of molecules that can be observed with this system to fairly rigid ones, but this limitation is much less at longer wavelengths where the density of states gets lower. While the current sensitivity of this first demonstration is not high enough for many applications, there are routes toward increasing the sensitivity with improved detection techniques and improved cavity mirrors. The combination of buffer-gas cooling with broadband THz spectroscopy could prove to be an interesting new tool for studying, for example, hydrogen bonding with higher resolution spectra and collisional relaxation of molecules with He and H_2 (which is of astrochemical relevance).

A common method for simplifying mass spectra is to add a temporal separation using gas chromatography (GC) [340, 341], which separates molecules based on their travel time through a long, narrow coated capillary tube, or column. Then, the time-dependent spectrum at the output of the column can consist of one, or a few, molecules instead of the original hundreds of molecules. GC is challenging to combine with spectroscopy because the sample volumes exiting the column are typically small and a moderately high time resolution is needed in order to take advantage of the time multiplexing offered by the GC. In addition, standard GC instruments are fairly large with significant electrical power requirements. Some microscale GC components have been fabricated since the 1970s; however, a fully chip-based micro-GC system was only recently demonstrated [342]. By combining this system with chip-based gas cells or miniature cavities as discussed in Section 4.C, the goal of GC-broadband spectroscopy might be achieved.

5. Conclusions

Broad-band spectroscopy with active light sources covers a wide range of technologies and spectrometer configurations, with different tradeoffs in sensitivity, wavelength coverage, and resolution. Newer laser-based sources provide higher spectral brightness, which enables high sensitivity with higher resolution, but with added complexity and the potential of added noise. Broadband spectrometers have already been used for a number of applications, including atmospheric trace gas measurements, breath analysis, kinetics studies, astrochemistry, industrial process monitoring, and fundamental laboratory spectroscopy. However, all of these applications could benefit from continued innovations in broadband spectroscopy, such as stronger light sources in certain wavelength regions (e.g. the mid-IR), more reflective and wider bandwidth mirrors to enable longer path lengths for cavity-enhanced measurements, and miniaturization for portability. With these continued advances in the base technology, we envision researchers will develop ever more capable broadband spectrometers leading to widespread adoption of this approach across medical diagnostics, atmospheric chemistry, combustion, research laboratories, and even future missions to other planets within the solar system.

Acknowledgments

KCC and EMW are supported by National Research Council postdoctoral fellowships. EMW thanks Kyle Zarzana for discussions about IBB-CES. The authors thank Thinh Bui, Steve Brown, Scott Diddams and Ian Coddington for useful discussions. This work was funded by DARPA DSO SCOUT program and the NIST greenhouse gas initiative.

References

1. Fraunhofer, J. Denkschriften der Königlichen Akademie der Wissenschaften zu München für das Jahr 1814 und 1815. Vol. 5. Bayerische Akademie der Wissenschaften; München: 1817. Bestimmung des Brechungs- und des Farben-Zerstreuungs - Vermögens verschiedener Glasarten, in Bezug auf die Vervollkommnung achromatischer Fernröhre; p. 193-226.
2. Brand, JCD. Lines of Light: The Sources of Dispersive Spectroscopy, 1800–1930. Gordon & Breach Publ; 1995.
3. Tennyson J, Bernath PF, Campargue A, Császár AG, Daumont L, Gamache RR, Hodges JT, Lisak D, Naumenko OV, Rothman LS, Tran H, Zobov NF, Buldyreva J, Boone CD, De VMD, Gianfrani L, Hartmann JM, McPheat R, Weidmann D, Murray J, Ngo NH, Polyansky OL. Recommended

isolated-line profile for representing high-resolution spectroscopic transitions (IUPAC Technical Report). Pure Appl Chem. 2014; 86:1931–1943.

4. Nozière B, Kalberer M, Claeys M, Allan J, D'Anna B, Decesari S, Finessi E, Glasius M, Grgić I, Hamilton JF, Hoffmann T, Iinuma Y, Jaoui M, Kahnt A, Kampf CJ, Kourtchev I, Maenhaut W, Marsden N, Saarikoski S, Schnelle-Kreis J, Surratt JD, Szidat S, Szmigielski R, Wisthaler A. The Molecular Identification of Organic Compounds in the Atmosphere: State of the Art and Challenges. Chem Rev. 2015; 115:3919–3983. [PubMed: 25647604]
5. Smith ML, Kort EA, Karion A, Sweeney C, Herndon SC, Yacovitch TI. Airborne Ethane Observations in the Barnett Shale: Quantification of Ethane Flux and Attribution of Methane Emissions. Environ Sci Technol. 2015; 49:8158–8166. [PubMed: 26148554]
6. Miller DJ, Sun K, Tao L, Pan D, Zondlo MA, Nowak JB, Liu Z, Diskin G, Sachse G, Beyersdorf A, Ferrare R, Scarino AJ. Ammonia and methane dairy emission plumes in the San Joaquin Valley of California from individual feedlot to regional scales. J Geophys Res Atmos. 2015; 120:9718–9738.
7. Mays KL, Shepson PB, Stirm BH, Karion A, Sweeney C, Gurney KR. Aircraft-Based Measurements of the Carbon Footprint of Indianapolis. Environ Sci Technol. 2009; 43:7816–7823. [PubMed: 19921899]
8. Karion A, Sweeney C, Pétron G, Frost G, Michael Hardesty R, Kofler J, Miller BR, Newberger T, Wolter S, Banta R, Brewer A, Dlugokencky E, Lang P, Montzka SA, Schnell R, Tans P, Trainer M, Zamora R, Conley S. Methane emissions estimate from airborne measurements over a western United States natural gas field. Geophys Res Lett. 2013; 40:4393–4397.
9. Karion A, Sweeney C, Kort EA, Shepson PB, Brewer A, Cambaliza M, Conley SA, Davis K, Deng A, Hardesty M, Herndon SC, Lauvaux T, Lavoie T, Lyon D, Newberger T, Pétron G, Rella C, Smith M, Wolter S, Yacovitch TI, Tans P. Aircraft-Based Estimate of Total Methane Emissions from the Barnett Shale Region. Environ Sci Technol. 2015; 49:8124–8131. [PubMed: 26148550]
10. Lavoie TN, Shepson PB, Cambaliza MOL, Stirm BH, Karion A, Sweeney C, Yacovitch TI, Herndon SC, Lan X, Lyon D. Aircraft-Based Measurements of Point Source Methane Emissions in the Barnett Shale Basin. Environ Sci Technol. 2015; 49:7904– 7913. [PubMed: 26148549]
11. Cicerone RJ, Oremland RS. Biogeochemical aspects of atmospheric methane. Glob Biogeochem Cycles. 1988; 2:299–327.
12. Schaefer H, Fletcher SEM, Veidt C, Lassey KR, Brailsford GW, Bromley TM, Dlugokencky EJ, Michel SE, Miller JB, Levin I, Lowe DC, Martin RJ, Vaughn BH, White JWC. A 21st-century shift from fossil-fuel to biogenic methane emissions indicated by $^{13}CH_4$. Science. 2016; 352:80–84. [PubMed: 26966190]
13. Webster CR, Heymsfield AJ. Water Isotope Ratios D/H, $^{18}O/^{16}O$, $^{17}O/^{16}O$ in and out of Clouds Map Dehydration Pathways. Science. 2003; 302:1742–1745. [PubMed: 14657493]
14. Gat JR. Oxygen and Hydrogen Isotopes in the Hydrologic Cycle. Annu Rev Earth Planet Sci. 1996; 24:225– 262.
15. Araguás-Araguás L, Froehlich K, Rozanski K. Deuterium and oxygen-18 isotope composition of precipitation and atmospheric moisture. Hydrol Process. 2000; 14:1341–1355.
16. Webster CR, Mahaffy PR, Flesch GJ, Niles PB, Jones JH, Leshin LA, Atreya SK, Stern JC, Christensen LE, Owen T, Franz H, Pepin RO, Steele A. tMS Team. Isotope Ratios of H, C, and O in CO_2 and H_2O of the Martian Atmosphere. Science. 2013; 341:260–263. [PubMed: 23869013]
17. Baldocchi DD, Hincks BB, Meyers TP. Measuring Biosphere-Atmosphere Exchanges of Biologically Related Gases with Micrometeorological Methods. Ecology. 1988; 69:1331–1340.
18. Fairall CW, White AB, Edson JB, Hare JE. Integrated Shipboard Measurements of the Marine Boundary Layer. J Atmos Oceanic Technol. 1997; 14:338–359.
19. Edson JB, Hinton AA, Prada KE, Hare JE, Fairall CW. Direct Covariance Flux Estimates from Mobile Platforms at Sea. J Atmos Oceanic Technol. 1998; 15:547–562.
20. Aubinet, M.Vesala, T., Papale, D., editors. Eddy Covariance: A Practical Guide to Measurement and Data Analysis. Springer Netherlands; Dordrecht: 2012.
21. Coburn S, Ortega I, Thalman R, Blomquist B, Fairall CW, Volkamer R. Measurements of diurnal variations and eddy covariance (EC) fluxes of glyoxal in the tropical marine boundary layer: Description of the Fast LED-CE-DOAS instrument. Atmos Meas Tech. 2014; 7:3579–3595.

22. Washenfelder RA, Flores JM, Brock CA, Brown SS, Rudich Y. Broadband measurements of aerosol extinction in the ultraviolet spectral region. Atmos Meas Tech. 2013; 6:861–877.
23. Finlayson-Pitts, BJ., Pitts, JN. Chemistry of the Upper and Lower Atmosphere: Theory, Experiments, and Applications. Academic Press; 1999.
24. Platt, U., Stutz, J. Physics of Earth and Space Environments. Springer; Berlin Heidelberg: 2008. Differential Absorption Spectroscopy.
25. Seinfeld, JH., Pandis, SN. Atmospheric Chemistry and Physics: From Air Pollution to Climate Change. Wiley; 2006.
26. Gilman JB, Lerner BM, Kuster WC, de Gouw JA. Source Signature of Volatile Organic Compounds from Oil and Natural Gas Operations in Northeastern Colorado. Environ Sci Technol. 2013; 47:1297– 1305. [PubMed: 23316938]
27. Atkinson R, Baulch DL, Cox RA, Crowley JN, Hampson RF, Hynes RG, Jenkin ME, Rossi MJ, Troe J. Evaluated kinetic and photochemical data for atmospheric chemistry: Volume I - gas phase reactions of Ox, HOx, NOx and SOx species. Atmos Chem Phys. 2004; 4:1461–1738.
28. Atkinson R, Baulch DL, Cox RA, Crowley JN, Hampson RF, Hynes RG, Jenkin ME, Rossi MJ, Troe J, Subcommittee IUPAC. Evaluated kinetic and photochemical data for atmospheric chemistry: Volume II – gas phase reactions of organic species. Atmos Chem Phys. 2006; 6:3625–4055.
29. Smith IWM. Laboratory Astrochemistry: Gas-Phase Processes. Annu Rev Astron Astrophys. 2011; 49:29–66.
30. Westbrook CK, Dryer FL. Chemical kinetic modeling of hydrocarbon combustion. Progress in Energy and Combustion Science. 1984; 10:1–57.
31. Westbrook CK. Chemical kinetics of hydrocarbon ignition in practical combustion systems. Proceedings of the Combustion Institute. 2000; 28:1563–1577.
32. Simmie JM. Detailed chemical kinetic models for the combustion of hydrocarbon fuels. Progress in Energy and Combustion Science. 2003; 29:599–634.
33. Battin-Leclerc F. Detailed chemical kinetic models for the low-temperature combustion of hydrocarbons with application to gasoline and diesel fuel surrogates. Progress in Energy and Combustion Science. 2008; 34:440– 498.
34. Zádor J, Taatjes CA, Fernandes RX. Kinetics of elementary reactions in low-temperature autoignition chemistry. Progress in Energy and Combustion Science. 2011; 37:371–421.
35. Seakins PW, Blitz MA. Developments in laboratory studies of gas-phase reactions for atmospheric chemistry with applications to isoprene oxidation and carbonyl chemistry. Annu Rev Phys Chem. 2011; 62:351– 373. [PubMed: 21219141]
36. Paulot F, Crounse JD, Kjaergaard HG, Kürten A, Clair JMS, Seinfeld JH, Wennberg PO. Unexpected Epoxide Formation in the Gas-Phase Photooxidation of Isoprene. Science. 2009; 325:730–733. [PubMed: 19661425]
37. Thalman, R. Phd. University of Colorado; Boulder: 2013. Development of Cavity Ehanced Differential Optical Absorption Spectroscopy (CE-DOAS) and application to laboratory and field measurements of trace gases and aerosols.
38. Hasson AS, Tyndall GS, Orlando JJ, Singh S, Hernandez SQ, Campbell S, Ibarra Y. Branching Ratios for the Reaction of Selected Carbonyl-Containing Peroxy Radicals with Hydroperoxy Radicals. J Phys Chem A. 2012; 116:6264–6281. [PubMed: 22483091]
39. Orlando JJ, Tyndall GS. Laboratory studies of organic peroxy radical chemistry: An overview with emphasis on recent issues of atmospheric significance. Chem Soc Rev. 2012; 41:6294–6317. [PubMed: 22847633]
40. Ahrens J, Carlsson PTM, Hertl N, Olzmann M, Pfeifle M, Wolf JL, Zeuch T. Infrared Detection of Criegee Intermediates Formed during the Ozonolysis of β-Pinene and Their Reactivity towards Sulfur Dioxide. Angew Chem Int Ed. 2014; 53:715–719.
41. Fleisher AJ, Bjork BJ, Bui TQ, Cossel KC, Okumura M, Ye J. Mid-Infrared Time-Resolved Frequency Comb Spectroscopy of Transient Free Radicals. J Phys Chem Lett. 2014; 5:2241–2246. [PubMed: 26279541]

42. Bjork BJ, Bui TQ, Heckl OH, Changala PB, Spaun B, Heu P, Follman D, Deutsch C, Cole GD, Aspelmeyer M, Okumura M, Ye J. Direct frequency comb measurement of OD + CO → DOCO kinetics. Science. 2016; 354:444–448. [PubMed: 27789837]
43. Miekisch W, Schubert JK, Noeldge-Schomburg GFE. Diagnostic potential of breath analysis—focus on volatile organic compounds. Clinica Chimica Acta. 2004; 347:25–39.
44. Buszewski B, Kesy M, Ligor T, Amann A. Human exhaled air analytics: Biomarkers of diseases. Biomed Chromatogr. 2007; 21:553–566. [PubMed: 17431933]
45. Cao W, Duan Y. Current Status of Methods and Techniques for Breath Analysis. Crit Rev Anal Chem. 2007; 37:3–13.
46. McCurdy MR, Bakhirkin Y, Wysocki G, Lewicki R, Tittel FK. Recent advances of laser-spectroscopy-based techniques for applications in breath analysis. J Breath Res. 2007; 1:014001. [PubMed: 21383427]
47. Risby TH. Critical issues for breath analysis. J Breath Res. 2008; 2:030302.
48. Wang C, Sahay P. Breath Analysis Using Laser Spectroscopic Techniques: Breath Biomarkers, Spectral Fingerprints, and Detection Limits. Sensors. 2009; 9:8230–8262. [PubMed: 22408503]
49. Simon, MG., Davis, CE. Instrumentation and Sensors for Human Breath Analysis. In: Mukhopadhyay, SC., Lay-Ekuakille, A., editors. Advances in Biomedical Sensing, Measurements, Instrumentation and Systems. Springer; Berlin Heidelberg: 2010. p. 144-165.no. 55 in Lecture Notes in Electrical Engineering
50. van de Kant KD, van der Sande LJ, Jöbsis Q, van Schayck OC, Dompeling E. Clinical use of exhaled volatile organic compounds in pulmonary diseases: A systematic review. Respir Res. 2012; 13:117. [PubMed: 23259710]
51. Amann A, Miekisch W, Schubert J, Buszewski B, Ligor T, Jezierski T, Pleil J, Risby T. Analysis of Exhaled Breath for Disease Detection. Annu Rev Anal Chem. 2014; 7:455–482.
52. Shorter JH, Nelson DD, McManus JB, Zahniser MS, Sama S, Milton DK. Clinical study of multiple breath biomarkers of asthma and COPD (NO, CO_2, CO and N_2O) by infrared laser spectroscopy. J Breath Res. 2011; 5:037108. [PubMed: 21757803]
53. Schwarz K, Pizzini A, Arendacká B, Zerlauth K, Filipiak W, Schmid A, Dzien A, Neuner S, Lechleitner M, Scholl-Bürgi S, Miekisch W, Schubert J, Unterkofler K, Witkovský V, Gastl G, Amann A. Breath acetone—aspects of normal physiology related to age and gender as determined in a PTR-MS study. J Breath Res. 2009; 3:027003. [PubMed: 21383458]
54. Mochalski P, King J, Klieber M, Unterkofler K, Hinterhuber H, Baumann M, Amann A. Blood and breath levels of selected volatile organic compounds in healthy volunteers. The Analyst. 2013; 138:2134. [PubMed: 23435188]
55. de Lacy Costello JBP, Ledochowski M, Ratcliffe NM. The importance of methane breath testing: A review. J Breath Res. 2013; 7:024001. [PubMed: 23470880]
56. Paredi P, Kharitonov SA, Leak D, Ward S, Cramer D, Barnes PJ. Exhaled ethane, a marker of lipid peroxidation, is elevated in chronic obstructive pulmonary disease. Am J Respir Crit Care Med. 2000; 162:369–373. [PubMed: 10934055]
57. Sulway MJ, Malins JM. Acetone in diabetic ketoacidosis. The Lancet. 1970; 296:736–740.
58. Deng C, Zhang J, Yu X, Zhang W, Zhang X. Determination of acetone in human breath by gas chromatography–mass spectrometry and solid-phase microextraction with on-fiber derivatization. Journal of Chromatography B. 2004; 810:269–275.
59. Turner C, Walton C, Hoashi S, Evans M. Breath acetone concentration decreases with blood glucose concentration in type I diabetes mellitus patients during hypoglycaemic clamps. J Breath Res. 2009; 3:046004. [PubMed: 21386197]
60. Skeldon KD, McMillan LC, Wyse CA, Monk SD, Gibson G, Patterson C, France T, Long-bottom C, Padgett MJ. Application of laser spectroscopy for measurement of exhaled ethane in patients with lung cancer. Respiratory Medicine. 2006; 100:300–306. [PubMed: 16002272]
61. Narasimhan LR, Goodman W, Patel CKN. Correlation of breath ammonia with blood urea nitrogen and creatinine during hemodialysis. Proc Natl Acad Sci. 2001; 98:4617–4621. [PubMed: 11296293]

62. Popa C, Dutu DCA, Cernat R, Matei C, Bratu AM, Banita S, Dumitras DC. Ethylene and ammonia traces measurements from the patients' breath with renal failure via LPAS method. Appl Phys B. 2011; 105:669–674.
63. Rubin T, von Haimberger T, Helmke A, Heyne K. Quantitative determination of metabolization dynamics by a real-time $^{13}CO_2$ breath test. J Breath Res. 2011; 5:027102. [PubMed: 21502704]
64. Lalazar G, Adar T, Ilan Y. Point-of-care continuous ^{13}C-methacetin breath test improves decision making in acute liver disease: Results of a pilot clinical trial. World J Gastroenterol. 2009; 15:966–972. [PubMed: 19248196]
65. Phillips M, Cataneo RN, Condos R, Ring Erickson GA, Greenberg J, La Bombardi V, Munawar MI, Tietje O. Volatile biomarkers of pulmonary tuberculosis in the breath. Tuberculosis. 2007; 87:44–52. [PubMed: 16635588]
66. Haick H, Broza YY, Mochalski P, Ruzsanyi V, Amann A. Assessment, origin, and implementation of breath volatile cancer markers. Chem Soc Rev. 2014; 43:1423–1449. [PubMed: 24305596]
67. Krilaviciute A, Heiss JA, Leja M, Kupcinskas J, Haick H, Brenner H. Detection of cancer through exhaled breath: A systematic review. Oncotarget. 2015; 6:38643–38657. [PubMed: 26440312]
68. Corradi M, Rubinstein I, Andreoli R, Manini P, Caglieri A, Poli D, Alinovi R, Mutti A. Aldehydes in exhaled breath condensate of patients with chronic obstructive pulmonary disease. Am J Respir Crit Care Med. 2003; 167:1380–1386. [PubMed: 12522029]
69. Smith MD. Spacecraft Observations of the Martian Atmosphere. Annu Rev Earth Planet Sci. 2008; 36:191– 219.
70. Coustenis A, Salama A, Schulz B, Ott S, Lellouch E, Encrenaz Th, Gautier D, Feuchtgruber H. Titan's atmosphere from ISO mid-infrared spectroscopy. Icarus. 2003; 161:383–403.
71. Roe HG. Titan's Methane Weather. Annu Rev Earth Planet Sci. 2012; 40:355–382.
72. Tokunaga AT. High-resolution infrared spectroscopy of planetary atmospheres. PASP. 1983; 95:691.
73. Tian F. Atmospheric Escape from Solar System Terrestrial Planets and Exoplanets. Annu Rev Earth Planet Sci. 2015; 43:459–476.
74. Wordsworth RD. The Climate of Early Mars. Annu Rev Earth Planet Sci. 2016; 44:381–408.
75. Mitchell JL, Lora JM. The Climate of Titan. Annu Rev Earth Planet Sci. 2016; 44:353–380.
76. Mahaffy PR, Webster CR, Atreya SK, Franz H, Wong M, Conrad PG, Harpold D, Jones JJ, Leshin LA, Manning H, Owen T, Pepin RO, Squyres S, Trainer M, Team MS. Abundance and Isotopic Composition of Gases in the Martian Atmosphere from the Curiosity Rover. Science. 2013; 341:263–266. [PubMed: 23869014]
77. Niles PB, Boynton WV, Hoffman JH, Ming DW, Hamara D. Stable isotope measurements of martian atmospheric CO_2 at the Phoenix landing site. Science. 2010; 329:1334–1337. [PubMed: 20829484]
78. Snow TP, McCall BJ. Diffuse Atomic and Molecular Clouds. Annu Rev Astron Astrophys. 2006; 44:367–414.
79. Snow TP, Bierbaum VM. Ion Chemistry in the Interstellar Medium. Annu Rev Anal Chem. 2008; 1:229–259.
80. Tielens AGGM. Interstellar Polycyclic Aromatic Hydrocarbon Molecules. Annu Rev Astron Astrophys. 2008; 46:289–337.
81. Herbst E, van Dishoeck EF. Complex Organic Interstellar Molecules. Annu Rev Astron Astrophys. 2009; 47:427–480.
82. Sarre PJ. The diffuse interstellar bands: A major problem in astronomical spectroscopy. Journal of Molecular Spectroscopy. 2006; 238:1–10.
83. Maier JP, Walker GAH, Bohlender DA, Mazzotti FJ, Raghunandan R, Fulara J, Garkusha I, Nagy A. Identification of H_2CCC as a Diffuse Interstellar Band Carrier. Ap J. 2011; 726:41.
84. Campbell EK, Holz M, Gerlich D, Maier JP. Laboratory confirmation of C_{60}^+ as the carrier of two diffuse interstellar bands. Nature. 2015; 523:322–323. [PubMed: 26178962]
85. Sims IR, Smith IWM. Gas-Phase Reactions and Energy Transfer at Very Low Temperatures. Annu Rev Phys Chem. 1995; 46:109–138. [PubMed: 24329120]

86. Smith IWM. Reactions at Very Low Temperatures: Gas Kinetics at a New Frontier. Angewandte Chemie International Edition. 2006; 45:2842–2861. [PubMed: 16628767]

87. Wakelam V, Herbst E, Loison J-C, Smith IWM, Chandrasekaran V, Pavone B, Adams NG, Bacchus-Montabonel M-C, Bergeat A, Béroff K, Bierbaum VM, Chabot M, Dalgarno A, van Dishoeck EF, Faure A, Geppert WD, Gerlich D, Galli D, Hébrard E, Hersant F, Hickson KM, Honvault P, Klippenstein SJ, Picard SL, Nyman G, Pernot P, Schlemmer S, Selsis F, Sims IR, Talbi D, Tennyson J, Troe J, Wester R, Wiesenfeld L. A KInetic Database for Astrochemistry (KIDA). ApJS. 2012; 199:21.

88. Lehman SY, Bertness KA, Hodges JT. Detection of trace water in phosphine with cavity ring-down spectroscopy. Journal of Crystal Growth. 2003; 250:262–268.

89. Funke HH, Grissom BL, McGrew CE, Raynor MW. Techniques for the measurement of trace moisture in high-purity electronic specialty gases. Rev Sci Instrum. 2003; 74:3909–3933.

90. Funke HH, Raynor MW, Bertness KA, Chen Y. Detection of Trace Water Vapor in High-Purity Phosphine Using Cavity Ring-down Spectroscopy. Appl Spectrosc. 2007; 61:419–423. [PubMed: 17456261]

91. Feng J, Clement R, Raynor M. Characterization of high-purity arsine and gallium arsenide epilayers grown by MOCVD. Journal of Crystal Growth. 2008; 310:4780–4785.

92. Cossel K, Adler F, Bertness K, Thorpe M, Feng J, Raynor M, Ye J. Analysis of trace impurities in semiconductor gas via cavity-enhanced direct frequency comb spectroscopy. Appl Phys B. 2010; 100:917–924.

93. Schroeder PJ, Wright RJ, Coburn S, Sodergren B, Cossel KC, Droste S, Truong GW, Baumann E, Giorgetta FR, Coddington I, Newbury NR, Rieker GB. Dual frequency comb laser absorption spectroscopy in a 16 MW gas turbine exhaust. Proceedings of the Combustion Institute. 2016

94. Rothman LS, Gordon IE, Babikov Y, Barbe A, Chris Benner D, Bernath PF, Birk M, Bizzocchi L, Boudon V, Brown LR, Campargue A, Chance K, Cohen EA, Coudert LH, Devi VM, Drouin BJ, Fayt A, Flaud JM, Gamache RR, Harrison JJ, Hartmann JM, Hill C, Hodges JT, Jacquemart D, Jolly A, Lamouroux J, Le Roy RJ, Li G, Long DA, Lyulin OM, Mackie CJ, Massie ST, Mikhailenko S, Müller HSP, Naumenko OV, Nikitin AV, Orphal J, Perevalov V, Perrin A, Polovtseva ER, Richard C, Smith MAH, Starikova E, Sung K, Tashkun S, Tennyson J, Toon GC, Tyuterev VG, Wagner G. The HITRAN 2012 molecular spectroscopic database. J Quant SpectroscRadiat Transfer. 2013; 130:4–50.

95. Rothman LS, Gordon IE, Barber RJ, Dothe H, Gamache RR, Goldman A, Perevalov VI, Tashkun SA, Tennyson J. HITEMP, the high-temperature molecular spectroscopic database. Journal of Quantitative Spectroscopy and Radiative Transfer. 2010; 111:2139–2150.

96. Keller-Rudek H, Moortgat GK, Sander R, Sörensen R. The MPI-Mainz UV/VIS Spectral Atlas of Gaseous Molecules of Atmospheric Interest. Earth Syst Sci Data. 2013; 5:365–373.

97. Chu PM, Guenther FR, Rhoderick GC, Lafferty WJ. The NIST quantitative infrared database. J Res Natl Inst Stand Technol. 1999; 104:59.

98. Sharpe SW, Johnson TJ, Sams RL, Chu PM, Rhoderick GC, Johnson PA. Gas-Phase Databases for Quantitative Infrared Spectroscopy. Appl Spectrosc. 2004; 58:1452–1461. [PubMed: 15606959]

99. Müller HSP, Thorwirth S, Roth DA, Winnewisser G. The Cologne Database for Molecular Spectroscopy, CDMS. Astron Astrophys. 2001; 370:L49–L52.

100. Müller HSP, Schlöder F, Stutzki J, Winnewisser G. The Cologne Database for Molecular Spectroscopy, CDMS: A useful tool for astronomers and spectroscopists. Journal of Molecular Structure. 2005; 742:215–227.

101. Pickett HM, Poynter RL, Cohen EA, Delitsky ML, Pearson JC, Müller HSP. Submillimeter, millimeter and microwave spectral line catalog. Journal of Quantitative Spectroscopy and Radiative Transfer. 1998; 60:883–890.

102. Jacquinet-Husson N, Armante R, Scott NA, Chédin A, Crépeau L, Boutammine C, Bouhdaoui A, Crevoisier C, Capelle V, Boonne C, Poulet-Crovisier N, Barbe A, Chris Benner D, Boudon V, Brown LR, Buldyreva J, Campargue A, Coudert LH, Devi VM, Down MJ, Drouin BJ, Fayt A, Fittschen C, Flaud JM, Gamache RR, Harrison JJ, Hill C, Hodnebrog O, Hu SM, Jacquemart D, Jolly A, Jiménez E, Lavrentieva NN, Liu AW, Lodi L, Lyulin OM, Massie ST, Mikhailenko S, Müller HSP, Naumenko OV, Nikitin A, Nielsen CJ, Orphal J, Perevalov VI, Perrin A, Polovtseva

E, Predoi-Cross A, Rotger M, Ruth AA, Yu SS, Sung K, Tashkun SA, Tennyson J, Tyuterev VG, Vander Auwera J, Voronin BA, Makie A. The 2015 edition of the GEISA spectroscopic database. Journal of Molecular Spectroscopy. 2016; 327:31–72.

103. Baumann E, Giorgetta FR, Swann WC, Zolot AM, Coddington I, Newbury NR. Spectroscopy of the methane ν_3 band with an accurate mid-infrared coherent dual-comb spectrometer. Phys Rev A. 2011; 84:062513.
104. Zolot A, Giorgetta F, Baumann E, Swann W, Coddington I, Newbury N. Broad-band frequency references in the near-infrared: Accurate dual comb spectroscopy of methane and acetylene. J Quant Spectrosc Radiat Transf. 2013; 118:26–39.
105. Okubo S, Iwakuni K, Inaba H, Hosaka K, Onae A, Sasada H, Hong F-L. Ultra-broadband dual-comb spectroscopy across 1.0–1.9 μm. Appl Phys Express. 2015; 8:082402.
106. Saykally RJ, Blake GA. Molecular Interactions and Hydrogen Bond Tunneling Dynamics: Some New Perspectives. Science. 1993; 259:1570–1575. [PubMed: 17733020]
107. Cole WTS, Farrell JD, Wales DJ, Saykally RJ. Structure and torsional dynamics of the water octamer from THz laser spectroscopy near 215 μm. Science. 2016; 352:1194–1197. [PubMed: 27257252]
108. Keutsch FN, Saykally RJ. Water clusters: Untangling the mysteries of the liquid, one molecule at a time. PNAS. 2001; 98:10533–10540. [PubMed: 11535820]
109. Crisp D, Atlas RM, Breon FM, Brown LR, Burrows JP, Ciais P, Connor BJ, Doney SC, Fung IY, Jacob DJ, Miller CE, O'Brien D, Pawson S, Randerson JT, Rayner P, Salawitch RJ, Sander SP, Sen B, Stephens GL, Tans PP, Toon GC, Wennberg PO, Wofsy SC, Yung YL, Kuang Z, Chudasama B, Sprague G, Weiss B, Pollock R, Kenyon D, Schroll S. The Orbiting Carbon Observatory (OCO) mission. Advances in Space Research. 2004; 34:700–709.
110. Bernath PF, McElroy CT, Abrams MC, Boone CD, Butler M, Camy-Peyret C, Carleer M, Clerbaux C, Coheur P-F, Colin R, DeCola P, De-Mazière M, Drummond JR, Dufour D, Evans WFJ, Fast H, Fussen D, Gilbert K, Jennings DE, Llewellyn EJ, Lowe RP, Mahieu E, McConnell JC, McHugh M, McLeod SD, Michaud R, Midwinter C, Nassar R, Nichitiu F, Nowlan C, Rinsland CP, Rochon YJ, Rowlands N, Semeniuk K, Simon P, Skelton R, Sloan JJ, Soucy M-A, Strong K, Tremblay P, Turnbull D, Walker KA, Walkty I, Wardle DA, Wehrle V, Zander R, Zou J. Atmospheric Chemistry Experiment (ACE): Mission overview. Geophys Res Lett. 2005; 32:L15S01.
111. Toon, G., Blavier, J-F., Washenfelder, R., Wunch, D., Keppel-Aleks, G., Wennberg, P., Connor, B., Sherlock, V., Griffith, D., Deutscher, N., Notholt, J. Advances in Imaging. Optical Society of America; 2009. Total Column Carbon Observing Network (TCCON); p. JMA3OSA Technical Digest (CD)
112. Wunch D, Toon GC, Blavier J-FL, Washenfelder RA, Notholt J, Connor BJ, Griffith DWT, Sherlock V, Wennberg PO. The Total Carbon Column Observing Network. Phil Trans R Soc A. 2011; 369:2087–2112. [PubMed: 21502178]
113. Haus R, Schäfer K, Bautzer W, Heland J, Mosebach H, Bittner H, Eisenmann T. Mobile Fourier-transform infrared spectroscopy monitoring of air pollution. Appl Opt. 1994; 33:5682. [PubMed: 20935969]
114. Wadsworth WJ, Joly N, Knight JC, Birks TA, Biancalana F, Russell PSJ. Supercontinuum and four-wave mixing with Q-switched pulses in endlessly single-mode photonic crystal fibres. Opt Express. 2004; 12:299. [PubMed: 19471538]
115. Alfano, RR., editor. The Supercontinuum Laser Source. Springer-Verlag; New York: 2006.
116. Genty G, Coen S, Dudley JM. Fiber super-continuum sources (Invited). J Opt Soc Am B. 2007; 24:1771.
117. Dudley, JM., Taylor, JR. Supercontinuum Generation in Optical Fibers. Cambridge University Press; 2010.
118. Savage N. Supercontinuum sources. Nat Photon. 2009; 3:114–115.
119. Kaminski CF, Watt RS, Elder AD, Frank JH, Hult J. Supercontinuum radiation for applications in chemical sensing and microscopy. Appl Phys B. 2008; 92:367.

120. Xia C, Kumar M, Kulkarni OR, Islam MN, Terry FL Jr, Freeman MJ. Mid-infrared supercontinuum generation to 4.5 μm in ZBLAN fluoride fibers by nanosecond diode pumping. Opt Lett. 2006; 31:2553– 2555. [PubMed: 16902616]

121. Kubat I, Agger CS, Møller U, Seddon AB, Tang Z, Sujecki S, Benson TM, Furniss D, Lamrini S, Scholle K, et al. Mid-infrared supercontinuum generation to 12.5 μm in large NA chalcogenide step-index fibres pumped at 4.5 μm. Opt Express. 2014; 22:19169–19182. [PubMed: 25321003]

122. Petersen CR, Møller U, Kubat I, Zhou B, Dupont S, Ramsay J, Benson T, Sujecki S, Abdel-Moneim N, Tang Z, Furniss D, Seddon A, Bang O. Mid-infrared supercontinuum covering the 1.4–13.3 μm molecular fingerprint region using ultra-high NA chalcogenide step-index fibre. Nat Photon. 2014; 8:830–834.

123. Jiang X, Joly NY, Finger MA, Babic F, Wong GKL, Travers JC, Russell PSJ. Deep-ultraviolet to mid-infrared supercontinuum generated in solid-core ZBLAN photonic crystal fibre. Nat Photon. 2015; 9:133–139.

124. Alfano, RR. The Supercontinuum Laser Source. Springer New York; New York, NY: 2016.

125. Newbury NR, Washburn BR, Corwin KL, Windeler RS. Noise amplification during supercontinuum generation in microstructure fiber. Opt Lett. 2002; 28:944–946.

126. Corwin KL, Newbury NR, Dudley JM, Coen S, Diddams SA, Washburn BR, Weber K, Windeler RS. Fundamental amplitude noise limitations to supercontinuum spectra generated in microstructure fiber. Appl Phys B. 2003; 77:269–277.

127. Dudley JM, Taylor JR. Ten years of nonlinear optics in photonic crystal fibre. Nat Photon. 2009; 3:85–90.

128. Møller U, Sørensen ST, Jakobsen C, Johansen J, Moselund PM, Thomsen CL, Bang O. Power dependence of supercontinuum noise in uniform and tapered PCFs. Opt Express. 2012; 20:2851. [PubMed: 22330522]

129. Møller U, Sørensen ST, Jakobsen C, Johansen J, Moselund PM, Thomsen CL, Bang O. Power dependence of supercontinuum noise in uniform and tapered PCFs: Erratum. Opt Express. 2012; 20:23318.

130. Langridge JM, Laurila T, Watt RS, Jones RL, Kaminski CF, Hult J. Cavity enhanced absorption spectroscopy of multiple trace gas species using a supercontinuum radiation source. Opt Express. 2008; 16:10178–10188. [PubMed: 18607425]

131. Woodward JT, Smith AW, Jenkins CA, Lin C, Brown SW, Lykke KR. Supercontinuum sources for metrology. Metrologia. 2009; 46:S277.

132. Godin T, Wetzel B, Sylvestre T, Larger L, Kudlinski A, Mussot A, Ben Salem A, Zghal M, Genty G, Dias F, Dudley JM. Real time noise and wavelength correlations in octave-spanning supercontinuum generation. Opt Express. 2013; 21:18452. [PubMed: 23938717]

133. Klimczak M, Soboń G, Kasztelanic R, Abramski KM, Buczyński R. Direct comparison of shot-to-shot noise performance of all normal dispersion and anomalous dispersion supercontinuum pumped with sub-picosecond pulse fiber-based laser. Sci Rep. 2016; 6:19284. [PubMed: 26759188]

134. Derickson, D. Fiber Optic Test and Measurement. Prentice Hall PTR; 1998.

135. Young, M. Optics and Lasers: Including Fibers and Optical Waveguides. Springer Science & Business Media; 2000.

136. Johnston PS, Lehmann KK. Cavity enhanced absorption spectroscopy using a broadband prism cavity and a supercontinuum source. Opt Express. 2008; 16:15013–15023. [PubMed: 18795038]

137. Michaels CA, Masiello T, Chu PM. Fourier Transform Spectrometry with a Near-Infrared Supercontinuum Source. Appl Spectrosc. 2009; 63:538–543. [PubMed: 19470210]

138. Aalto A, Genty G, Laurila T, Toivonen J. Incoherent broadband cavity enhanced absorption spectroscopy using supercontinuum and superluminescent diode sources. Opt Express. 2015; 23:25225. [PubMed: 26406720]

139. Werblinski T, Lämmlein B, Huber FJT, Zigan L, Will S. Supercontinuum high-speed cavity-enhanced absorption spectroscopy for sensitive multi-species detection. Opt Lett. 2016; 41:2322. [PubMed: 27176993]

140. Cundiff ST, Ye J. Colloquium: Femtosecond optical frequency combs. Rev Mod Phys. 2003; 75:325–342.

141. Adler F, Cossel KC, Thorpe MJ, Hartl I, Fermann ME, Ye J. Phase-stabilized, 1.5 W frequency comb at 2.8–4.8 μm. Opt Lett. 2009; 34:1330–1332. [PubMed: 19412262]
142. Maidment L, Schunemann PG, Reid DT. Molecular fingerprint-region spectroscopy from 5 to 12 μm using an orientation-patterned gallium phosphide optical parametric oscillator. Opt Lett. 2016; 41:4261. [PubMed: 27628372]
143. Smolski VO, Yang H, Gorelov SD, Schunemann PG, Vodopyanov KL. Coherence properties of a 2.6–7.5 μm frequency comb produced as a subharmonic of a Tm-fiber laser. Opt Lett. 2016; 41:1388. [PubMed: 27192243]
144. Heckl OH, Bjork BJ, Winkler G, Changala PB, Spaun B, Bui TQ, Lee KF, Jiang J, Fermann M, Schunemann PG, Jun Ye. Three Photon Absorption in Optical Parametric Oscillators Based on OP-GaAs. Opt Lett. 2016
145. Cruz FC, Maser DL, Johnson T, Ycas G, Klose A, Giorgetta FR, Coddington I, Diddams SA. Mid-infrared optical frequency combs based on difference frequency generation for molecular spectroscopy. Opt Express. 2015; 23:26814. [PubMed: 26480192]
146. Pupeza I, Sánchez D, Zhang J, Lilienfein N, Seidel M, Karpowicz N, Paasch-Colberg T, Znakovskaya I, Pescher M, Schweinberger W, Pervak V, Fill E, Pronin O, Wei Z, Krausz F, Apolonski A, Biegert J. High-power sub-two-cycle mid-infrared pulses at 100 MHz repetition rate. Nat Photon. 2015; 9:721– 724.
147. Maslowski, P., Cossel, KC., Foltynowicz, A., Ye, J. Cavity-Enhanced Spectroscopy and Sensing. Springer; Berlin Heidelberg: 2014. Cavity-enhanced direct frequency comb spectroscopy; p. 271-321.
148. Burrows JP, Richter A, Dehn A, Deters B, Himmelmann S, Voigt S, Orphal J. Atmospheric Remote-Sensing Reference Data from GOME-2. Temperature-Dependent Absorption Cross Sections of O_3 in the 231–794nm Range. Journal of Quantitative Spectroscopy and Radiative Transfer. 1999; 61:509–517.
149. Vandaele AC, Hermans C, Fally S, Carleer M, Colin R, Mérienne M-F, Jenouvrier A, Coquart B. High-resolution Fourier transform measurement of the NO_2 visible and near-infrared absorption cross sections: Temperature and pressure effects. J-Geophys- Res. 2002; 107:4348.
150. Yokelson RJ, Burkholder JB, Fox RW, Talukdar RK, Ravishankara AR. Temperature Dependence of the NO_3 Absorption Spectrum. J Phys Chem. 1994; 98:13144–13150.
151. Bartels A, Heinecke D, Diddams SA. 10-GHz Self-Referenced Optical Frequency Comb. Science. 2009; 326:681–681. [PubMed: 19900924]
152. Sinclair LC, Deschênes J-D, Sonderhouse L, Swann WC, Khader IH, Baumann E, Newbury NR, Coddington I. Invited Article: A compact optically coherent fiber frequency comb. Rev Sci Instrum. 2015; 86:081301. [PubMed: 26329167]
153. Faist J, Villares G, Scalari G, Rösch M, Bonzon C, Hugi A, Beck M. Quantum Cascade Laser Frequency Combs. Nanophotonics. 2016
154. Finneran IA, Good JT, Holland DB, Carroll PB, Allodi MA, Blake GA. Decade-spanning high-precision terahertz frequency comb. Phys Rev Lett. 2015; 114:163902. [PubMed: 25955051]
155. McManus JB, Kebabian PL, Zahniser MS. Astigmatic mirror multipass absorption cells for long-path-length spectroscopy. Appl Opt. 1995; 34:3336–3348. [PubMed: 21052141]
156. Silver JA. Simple dense-pattern optical multipass cells. Appl Opt. 2005; 44:6545–6556. [PubMed: 16270543]
157. Tuzson B, Mangold M, Looser H, Manninen A, Emmenegger L. Compact multipass optical cell for laser spectroscopy. Opt Lett. 2013; 38:257–259. [PubMed: 23381403]
158. Thorpe MJ, Ye J. Cavity-enhanced direct frequency comb spectroscopy. Appl Phys B. 2008; 91:397–414.
159. Romanini, D., Ventrillard, I., Méjean, G., Morville, J., Kerstel, E. Introduction to Cavity Enhanced Absorption Spectroscopy. In: Gagliardi, G., Loock, H-P., editors. Cavity-Enhanced Spectroscopy and Sensing. Springer; Berlin Heidelberg: 2014. p. 1-60.no. 179 in Springer Series in Optical Sciences
160. Fante RL. Electromagnetic beam propagation in turbulent media. Proc IEEE. 1975; 63:1669–1692.
161. Davis, SP., Abrams, MC., Brault, JW. Fourier Transform Spectrometry. Academic Press; 2001.

162. Griffiths, PR., Haseth, JA. Fourier Transform Infrared Spectrometry. Wiley-Interscience; 2007.
163. Diddams SA, Hollberg L, Mbele V. Molecular fingerprinting with the resolved modes of a femtosecond laser frequency comb. Nature. 2007; 445:627–630. [PubMed: 17287805]
164. Vogt SS, Allen SL, Bigelow BC, Bresee L, Brown WE, Cantrall T, Conrad A, Couture M, Delaney C, Epps HW, Hilyard D, Hilyard DF, Horn E, Jern N, Kanto D, Keane MJ, Kibrick RI, Lewis JW, Osborne J, Pardeilhan GH, Pfister T, Ricketts T, Robinson LB, Stover RJ, Tucker D, Ward JM, Wei M. HIRES: The high-resolution echelle spectrometer on the Keck 10-m Telescope. Proc SPIE. 1994; 2198:362–375.
165. Zolot AM, Giorgetta FR, Baumann E, Nicholson JW, Swann WC, Coddington I, Newbury NR. Direct-comb molecular spectroscopy with accurate, resolved comb teeth over 43 THz. Opt Lett. 2012; 37:638–640. [PubMed: 22344132]
166. Maslowski P, Lee KF, Johansson AC, Khodabakhsh A, Kowzan G, Rutkowski L, Mills AA, Mohr C, Jiang J, Fermann ME, Foltynowicz A. Surpassing the path-limited resolution of Fourier-transform spectrometry with frequency combs. Phys Rev A. 2016; 93:021802.
167. Tso T-L, Chang S-Y. Unambiguous Identification of Fugitive Pollutants and the Determination of Annual Emission Flux as a Diurnal Monitoring Mode Using Open-Path Fourier-Transform Infrared Spectroscopy. Anal Sci. 1996; 12:311–319.
168. Ball SM, Jones RL. Broad-Band Cavity Ring-Down Spectroscopy. Chem Rev. 2003; 103:5239–5262. [PubMed: 14664650]
169. Volkamer R, Molina LT, Molina MJ, Shirley T, Brune WH. DOAS measurement of glyoxal as an indicator for fast VOC chemistry in urban air. Geophys Res Lett. 2005; 32:L08806.
170. Thorpe MJ, Balslev-Clausen D, Kirchner MS, Ye J. Cavity-enhanced optical frequency combspectroscopy: Application to human breath analysis. Opt Express. 2008; 16:2387–2397. [PubMed: 18542317]
171. Thalman R, Volkamer R. Inherent calibration of a blue LED-CE-DOAS instrument to measure iodine oxide, glyoxal, methyl glyoxal, nitrogen dioxide, water vapour and aerosol extinction in open cavity mode. Atmos Meas Tech. 2010; 3:1797–1814.
172. Foltynowicz A, Maslowski P, Fleisher AJ, Bjork BJ, Ye J. Cavity-enhanced optical frequency comb spectroscopy in the mid-infrared application to trace detection of hydrogen peroxide. Appl Phys B. 2012; 110:163–175.
173. Grilli R, Méjean G, Abd Alrahman C, Ventrillard I, Kassi S, Romanini D. Cavity-enhanced multiplexed comb spectroscopy down to the photon shot noise. Phys Rev A. 2012; 85:051804.
174. Roy J, Deschênes J-D, Potvin S, Genest J. Continuous real-time correction and averaging for frequency comb interferometry. Opt Express. 2012; 20:21932– 21939. [PubMed: 23037343]
175. Khodabakhsh A, Alrahman CA, Foltynowicz A. Noise-immune cavity-enhanced optical frequency comb spectroscopy. Opt Lett. 2014; 39:5034. [PubMed: 25166067]
176. Rieker GB, Giorgetta FR, Swann WC, Kofler J, Zolot AM, Sinclair LC, Baumann E, Cromer C, Petron G, Sweeney C, Tans PP, Coddington I, Newbury NR. Frequency-comb-based remote sensing of greenhouse gases over kilometer air paths. Optica. 2014; 1:290–298.
177. Newbury NR, Coddington I, Swann WC. Sensitivity of coherent dual-comb spectroscopy. Opt Express. 2010; 18:7929–7945. [PubMed: 20588636]
178. Coddington I, Newbury N, Swann W. Dual-comb spectroscopy. Optica. 2016; 3:414.
179. Foltynowicz A, Ban T, Masłowski P, Adler F, Ye J. Quantum-Noise-Limited Optical Frequency Comb Spectroscopy. Phys Rev Lett. 2011; 107:233002. [PubMed: 22182084]
180. Hirschfeld T. The Implications of Fluctuation Noise in Multiplex Spectroscopy. Appl Spectrosc, AS. 1976; 30:234–236.
181. Fellgett, PB. Phd thesis. University of Cambridge; Cambridge, UK: 1951. The Multiplex Advantage.
182. Jacquinot, P. XVII Me Congrs Du GAMS. Paris: 1954. The Etendue Advantage.
183. Gebbie HA. Fourier transform spectroscopy—Recollections of the period 1955–1960. Infrared Physics. 1984; 24:105–109.
184. Connes P. Early history of fourier transform spectroscopy. Infrared Physics. 1984; 24:69–93.

185. Esler MB, Griffith DWT, Wilson SR, Steele LP. Precision Trace Gas Analysis by FT-IR Spectroscopy. 1. Simultaneous Analysis of CO_2, CH_4, N_2O, and CO in Air. Anal Chem. 2000; 72:206–215. [PubMed: 10655655]

186. Esler MB, Griffith DWT, Wilson SR, Steele LP. Precision Trace Gas Analysis by FT-IR Spectroscopy. 2. The $^{13}C/^{12}C$ Isotope Ratio of CO_2. Anal Chem. 2000; 72:216–221. [PubMed: 10655656]

187. Yost MG, Rose MA, Morgan MS. An Evaluation of Fourier Transform Infrared (FTIR) Spectroscopy for Detecting Organic Solvents in Expired Breath. Appl Occup Environ Hyg. 2003; 18:160–169. [PubMed: 12573961]

188. Marshall TL, Chaffin CT, Hammaker RM, Fateley WG. An introduction to open-path FT-IR atmospheric monitoring. Environ Sci Technol. 1994; 28:224A–232A.

189. Levine SP, Russwurm GM. Fourier transform infrared optical remote sensing for monitoring airborne gas and vapor contaminants in the field. TrAC Trends in Analytical Chemistry. 1994; 13:258–262.

190. Herget WF, Brasher JD. Remote measurement of gaseous pollutant concentrations using a mobile Fourier transform interferometer system. Appl Opt. 1979; 18:3404–3420. [PubMed: 20216620]

191. Fateley WG, Hammaker RM, Tucker MD, Witkowski MR, Chaffin CT, Marshall TL, Davis M, Thomas MJ, Arello J, Hudson JL, Fairless BJ. Observing industrial atmospheric environments by FT-IR. Journal of Molecular Structure. 1995; 347:153– 168.

192. Todd LA, Ramanathan M, Mottus K, Katz R, Dodson A, Mihlan G. Measuring chemical emissions using open-path Fourier transform infrared (OP-FTIR) spectroscopy and computer-assisted tomography. Atmospheric Environment. 2001; 35:1937–1947.

193. Childers JW, Thompson EL Jr, Harris DB, Kirchgessner DA, Clayton M, Natschke DF, Phillips WJ. Multi-pollutant concentration measurements around a concentrated swine production facility using open-path FTIR spectrometry. Atmospheric Environment. 2001; 35:1923–1936.

194. Gosz JR, Dahm CN, Risser PG. Long-Path FTIR Measurement of Atmospheric Trace Gas Concentrations. Ecology. 1988; 69:1326–1330.

195. Schütze C, Lau S, Reiche N, Sauer U, Borsdorf H, Dietrich P. Ground-based Remote Sensing with Open-path Fourier-transform Infrared (OP-FTIR) Spectroscopy for Large-scale Monitoring of Greenhouse Gases. Energy Procedia. 2013; 37:4276–4282.

196. Akagi SK, Burling IR, Mendoza A, Johnson TJ, Cameron M, Griffith DWT, Paton-Walsh C, Weise DR, Reardon J, Yokelson RJ. Field measurements of trace gases emitted by prescribed fires in southeastern US pine forests using an open-path FTIR system. Atmos Chem Phys. 2014; 14:199–215.

197. Carter RE, Thomas MJ, Marotz GA, Lane DD, Hudson JL. Compound detection and concentration estimation by open-path Fourier Transform Infrared Spectrometry and canisters under controlled field conditions. Environ Sci Technol. 1992; 26:2175–2181.

198. Smith TEL, Wooster MJ, Tattaris M, Griffith DWT. Absolute accuracy and sensitivity analysis of OP-FTIR retrievals of CO_2, CH_4 and CO over concentrations representative of “clean air” and “polluted plumes. Atmos Meas Tech. 2011; 4:97–116.

199. Eberhard J, Yeh P-S, Lee Y-P. Laser-photolysis/time-resolved Fourier-transform absorption spectroscopy: Formation and quenching of HCl(v) in the chain reaction $Cl/Cl_2/H_2$. J Chem Phys. 1997; 107:6499–6502.

200. Hartland GV, Xie W, Dai H-L, Simon A, Anderson MJ. Time-resolved Fourier transform spectroscopy with 0.25 cm^{-1} spectral and $<10^{-7}$ s time resolution in the visible region. Rev Sci Instrum. 1992; 63:3261–3267.

201. Hatakeyama S, Akimoto H. Reactions of Criegee intermediates in the gas phase. Res Chem Intermed. 1994; 20:503–524.

202. Mauldin RL III, Berndt T, Sipilä M, Paasonen P, Petäjä T, Kim S, Kurtén T, Stratmann F, Kerminen V-M, Kulmala M. A new atmospherically relevant oxidant of sulphur dioxide. Nature. 2012; 488:193– 196. [PubMed: 22874964]

203. Newland MJ, Rickard AR, Vereecken L, Muñoz A, Ródenas M, Bloss WJ. Atmospheric isoprene ozonolysis: Impacts of stabilised Criegee intermediate reactions with SO_2, H_2O and dimethyl sulfide. Atmos Chem Phys. 2015; 15:9521–9536.

204. Su Y-T, Lin H-Y, Putikam R, Matsui H, Lin MC, Lee Y-P. Extremely rapid self-reaction of the simplest Criegee intermediate CH_2OO and its implications in atmospheric chemistry. Nat Chem. 2014; 6:477–483. [PubMed: 24848232]
205. Lin H-Y, Huang Y-H, Wang X, Bowman JM, Nishimura Y, Witek HA, Lee Y-P. Infrared identification of the Criegee intermediates syn- and anti-CH_3CHOO, and their distinct conformation- dependent reactivity. Nat Commun. 2015; 6:7012. [PubMed: 25959902]
206. Mandon J, Guelachvili G, Picqué N, Druon F, Georges P. Femtosecond laser Fourier transform absorption spectroscopy. Opt Lett. 2007; 32:1677–1679. [PubMed: 17572744]
207. Mandon J, Sorokin E, Sorokina IT, Guelachvili G, Picqué N. Supercontinua for high-resolution absorption multiplex infrared spectroscopy. Opt Lett. 2008; 33:285–287. [PubMed: 18246156]
208. Mandon J, Guelachvili G, Picqué N. Fourier transform spectroscopy with a laser frequency comb. Nat Photon. 2009; 3:99–102.
209. Adler F, Maslowski P, Foltynowicz A, Cossel KC, Briles TC, Hartl I, Ye J. Mid-infrared Fourier transform spectroscopy with a broadband frequency comb. Opt Express. 2010; 18:21861. [PubMed: 20941086]
210. Fiedler SE, Hese A, Ruth AA. Incoherent broad-band cavity-enhanced absorption spectroscopy. Chemical Physics Letters. 2003; 371:284–294.
211. Min K-E, Washenfelder RA, Dubé WP, Langford AO, Edwards PM, Zarzana KJ, Stutz J, Lu K, Rohrer F, Zhang Y, Brown SS. A broadband cavity enhanced absorption spectrometer for aircraft measurements of glyoxal, methylglyoxal, nitrous acid, nitrogen dioxide, and water vapor. Atmos Meas Tech. 2016; 9:423–440.
212. Washenfelder RA, Langford AO, Fuchs H, Brown SS. Measurement of glyoxal using an incoherent broadband cavity enhanced absorption spectrometer. Atmos Chem Phys. 2008; 8:7779–7793.
213. Axson JL, Washenfelder RA, Kahan TF, Young CJ, Vaida V, Brown SS. Absolute ozone absorption cross section in the Huggins Chappuis minimum (350–470 nm) at 296 K. Atmos Chem Phys. 2011; 11:11581–11590.
214. Langridge JM, Ball SM, Jones RL. A compact broadband cavity enhanced absorption spectrometer for detection of atmospheric NO_2 using light emitting diodes. The Analyst. 2006; 131:916. [PubMed: 17028725]
215. Kennedy OJ, Ouyang B, Langridge JM, Daniels MJS, Bauguitte S, Freshwater R, McLeod MW, Ironmonger C, Sendall J, Norris O, Nightingale R, Ball SM, Jones RL. An aircraft based three channel broadband cavity enhanced absorption spectrometer for simultaneous measurements of NO_3, N_2O_5 and NO_2. Atmospheric Meas Tech. 2011; 4:1759–1776.
216. Washenfelder RA, Young CJ, Brown SS, Angevine WM, Atlas EL, Blake DR, Bon DM, Cubison MJ, de Gouw JA, Dusanter S, Flynn J, Gilman JB, Graus M, Griffith S, Grossberg N, Hayes PL, Jimenez JL, Kuster WC, Lefer BL, Pollack IB, Ryerson TB, Stark H, Stevens PS, Trainer MK. The glyoxal budget and its contribution to organic aerosol for Los Angeles, California, during CalNex 2010: Glyoxal budget for Loas Angeles. J Geophys Res Atmospheres. 2011; 116
217. Thalman R, Volkamer R. Temperature dependent absorption cross-sections of O_2–O_2 collision pairs between 340 and 630 nm and at atmospherically relevant pressure. Phys Chem Chem Phys. 2013; 15:15371. [PubMed: 23928555]
218. Ball SM, Langridge JM, Jones RL. Broadband cavity enhanced absorption spectroscopy using light emitting diodes. Chemical Physics Letters. 2004; 398:68–74.
219. Vaughan S, Gherman T, Ruth AA, Orphal J. Incoherent broad-band cavity-enhanced absorption spectroscopy of the marine boundary layer species $I_{2,\ IO\ and\ OIO}$. Phys Chem Chem Phys. 2008; 10:4471– 4477. [PubMed: 18654688]
220. Langridge JM, Ball SM, Shillings AJL, Jones RL. A broadband absorption spectrometer using light emitting diodes for ultrasensitive, in situ trace gas detection. Rev Sci Instrum. 2008; 79:123110. [PubMed: 19123548]
221. Triki M, Cermak P, Méjean G, Romanini D. Cavity-enhanced absorption spectroscopy with a red LED source for NOx. Appl Phys B. 2008; 91:195–201.

222. Washenfelder RA, Attwood AR, Flores JM, Zarzana KJ, Rudich Y, Brown SS. Broadband cavity-enhanced absorption spectroscopy in the ultraviolet spectral region for measurements of nitrogen dioxide and formaldehyde. Atmos Meas Tech. 2016; 9:41–52.

223. Platt, U., Perner, D. Measurements of Atmospheric Trace Gases by Long Path Differential UV/Visible Absorption Spectroscopy. In: Killinger, DDK., Mooradian, DA., editors. Optical and Laser Remote Sensing. Springer; Berlin Heidelberg: 1983. p. 97-105.no. 39 in Springer Series in Optical Sciences

224. Platt U, Perner D, Winer AM, Harris GW, Pitts JN. Detection of NO_3 in the polluted troposphere by differential optical absorption. Geophys Res Lett. 1980; 7:89–92.

225. Stutz J, Platt U. Improving long-path differential optical absorption spectroscopy with a quartz-fiber mode mixer. Appl Opt. 1997; 36:1105. [PubMed: 18250777]

226. Stutz J, Alicke B, Ackermann R, Geyer A, White A, Williams E. Vertical profiles of NO_3, N_2O_5, O_3, and NOx in the nocturnal boundary layer: 1. Observations during the Texas Air Quality Study 2000. J Geophys Res. 2004; 109:D12306.

227. Alicke B, Hebestreit K, Stutz J, Platt U. Iodine oxide in the marine boundary layer. Nature. 1999; 397:572– 573. [PubMed: 10050849]

228. Velasco E, Lamb B, Westberg H, Allwine E, Sosa G, Arriaga-Colina JL, Jobson BT, Alexander ML, Prazeller P, Knighton WB, Rogers TM, Grutter M, Herndon SC, Kolb CE, Zavala M, de Foy B, Volkamer R, Molina LT, Molina MJ. Distribution, magnitudes, reactivities, ratios and diurnal patterns of volatile organic compounds in the Valley of Mexico during the MCMA 2002 & 2003 field campaigns. Atmos Chem Phys. 2007; 7:329–353.

229. Wang S, Ackermann R, Stutz J. Vertical profiles of O_3 and NOx chemistry in the polluted nocturnal boundary layer in Phoenix, AZ: I. Field observations by long-path DOAS. Atmos Chem Phys. 2006; 6:2671– 2693.

230. Tsai C, Wong C, Hurlock S, Pikelnaya O, Mielke LH, Osthoff HD, Flynn JH, Haman C, Lefer B, Gilman J, de Gouw J, Stutz J. Nocturnal loss of NOx during the 2010 CalNex-LA study in the Los Angeles Basin. J Geophys Res Atmos. 2014; 119:13,004– 13,025.

231. O'Keefe A, Deacon DAG. Cavity ring-down optical spectrometer for absorption measurements using pulsed laser sources. Rev Sci Instrum. 1988; 59:2544– 2551.

232. Zarzana KJ, De Haan DO, Freedman MA, Hasenkopf CA, Tolbert MA. Optical Properties of the Products of α-Dicarbonyl and Amine Reactions in Simulated Cloud Droplets. Environ Sci Technol. 2012; 46:4845–4851. [PubMed: 22515474]

233. Engeln R, Meijer G. A Fourier transform cavity ring down spectrometer. Rev Sci Instrum. 1996; 67:2708– 2713.

234. Scherer JJ. Ringdown spectral photography. Chemical Physics Letters. 1998; 292:143–153.

235. Ball SM, Povey IM, Norton EG, Jones RL. Broadband cavity ringdown spectroscopy of the NO_3 radical. Chemical Physics Letters. 2001; 342:113–120.

236. Thorpe MJ, Moll KD, Jones RJ, Safdi B, Ye J. Broadband Cavity Ringdown Spectroscopy for Sensitive and Rapid Molecular Detection. Science. 2006; 311:1595–1599. [PubMed: 16543457]

237. Gherman T, Romanini D. Mode–locked cavity–enhanced absorption spectroscopy. Opt Express. 2002; 10:1033–1042. [PubMed: 19451961]

238. Villa M, Fusina L, Lonardo GD, d'Elseghem Vaernewijck XDG, Herman M. Femto-FT-CEAS investigation of rare acetylene isotopologues ($H^{12}C^{13}CD$, $D^{12}C^{13}H$ and $D^{12}C^{13}D$). Mol Phys. 2013; 111:1972–1976.

239. Bernhardt B, Ozawa A, Jacquet P, Jacquey M, Kobayashi Y, Udem T, Holzwarth R, Guelachvili G, Hänsch TW, Picqué N. Cavity-enhanced dual-comb spectroscopy. Nature Photon. 2010; 4:55–57.

240. Fleisher AJ, Long DA, Reed ZD, Hodges JT, Plusquellic DF. Coherent cavity-enhanced dual-comb spectroscopy. Opt Express. 2016; 24:10424. [PubMed: 27409866]

241. Grilli R, Méjean G, Kassi S, Ventrillard I, Abd-Alrahman C, Romanini D. Frequency Comb Based Spectrometer for in Situ and Real Time Measurements of IO, BrO, NO_2, and H_2CO at pptv and ppqv Levels. Environ Sci Technol. 2012; 46:10704–10710. [PubMed: 22889080]

242. Grilli R, Legrand M, Kukui A, Méjean G, Preunkert S, Romanini D. First investigations of IO, BrO, and NO_2 summer atmospheric levels at a coastal East Antarctic site using mode-locked cavity enhanced absorption spectroscopy. Geophys Res Lett. 2013; 40:791– 796.

243. Coddington I, Swann WC, Newbury NR. Coherent dual-comb spectroscopy at high signal-to-noise ratio. Phys Rev A. 2010; 82:043817.

244. Schliesser A, Brehm M, Keilmann F, van der Weide D. Frequency-comb infrared spectrometer for rapid, remote chemical sensing. Opt Express. 2005; 13:9029–9038. [PubMed: 19498938]

245. Giorgetta FR, Rieker GB, Baumann E, Swann WC, Sinclair LC, Kofler J, Coddington I, Newbury NR. Broadband Phase Spectroscopy over Turbulent Air Paths. Phys Rev Lett. 2015; 115:103901. [PubMed: 26382677]

246. Nugent-Glandorf L, Giorgetta FR, Diddams SA. Open-air, broad-bandwidth trace gas sensing with a mid-infrared optical frequency comb. Appl Phys B. 2015; 119:327–338.

247. Iwakuni K, Okubo S, Yamada T, Inaba Koichi MH, Onae A, Hong F-L, Sasada H. Ortho-Para-Dependent Pressure Effects Observed in the Near Infrared Band of Acetylene by Dual-Comb Spectroscopy. Phys Rev Lett. 2016; 117:143902. [PubMed: 27740784]

248. Withayachumnankul W, Naftaly M. Fundamentals of measurement in terahertz time-domain spectroscopy. J Infrared Millim Terahertz Waves. 2014; 35:610–637.

249. Schmuttenmaer CA. Exploring dynamics in the far-infrared with terahertz spectroscopy. Chem Rev. 2004; 104:1759–1780. [PubMed: 15080711]

250. Bartels A, Cerna R, Kistner C, Thoma A, Hudert F, Janke C, Dekorsy T. Ultrafast time-domain spectroscopy based on high-speed asynchronous optical sampling. Rev Sci Instrum. 2007; 8:462.

251. Hsieh Y-D, Iyonaga Y, Sakaguchi Y, Yokoyama S, Inaba H, Minoshima K, Hindle F, Araki T, Yasui T. Spectrally interleaved, comb-mode-resolved spectroscopy using swept dual terahertz combs. Sci Rep. 2014; 4:3816. [PubMed: 24448604]

252. Auston D, Cheung K, Smith P. Picosecond photoconducting hertzian dipoles. Appl Phys Lett. 1984; 45:284–286.

253. Hale P, Madeo J, Chin C, Dhillon S, Mangeney J, Tignon J, Dani K. 20 THz broadband generation using semi-insulating gaas interdigitated photoconductive antennas. Opt Express. 2014; 22:26358–26364. [PubMed: 25401668]

254. Dreyhaupt A, Winnerl S, Dekorsy T, Helm M. High-intensity terahertz radiation from a microstructured large-area photoconductor. Appl Phys Lett. 2005; 86:121114.

255. Wu Q, Litz M, Zhang X-C. Broadband detection capability of ZnTe electro-optic field detectors. Appl Phys Lett. 1996; 68:2924–2926.

256. Wu Q, Zhang X-C. Free-space electro-optic sampling of terahertz beams. Appl Phys Lett. 1995; 67:3523– 3525.

257. Nahata A, Weling AS, Heinz TF. A wideband coherent terahertz spectroscopy system using optical rectification and electro-optic sampling. Appl Phys Lett. 1996; 69:2321–2323.

258. Hebling J, Almasi G, Kozma I, Kuhl J. Velocity matching by pulse front tilting for large area THz-pulse generation. Opt Express. 2002; 10:1161–1166. [PubMed: 19451975]

259. Sell A, Leitenstorfer A, Huber R. Phase-locked generation and field-resolved detection of widely tunable terahertz pulses with amplitudes exceeding 100 MV/cm. Opt Lett. 2008; 33:2767–2769. [PubMed: 19037420]

260. Ferguson B, Zhang X-C. Materials for terahertz science and technology. Nat Mater. 2002; 1:26–33. [PubMed: 12618844]

261. Vicario C, Jazbinsek M, Ovchinnikov A, Chefonov O, Ashitkov S, Agranat M, Hauri C. High efficiency THz generation in DSTMS, DAST and OH1 pumped by Cr: forsterite laser. Opt Express. 2015; 23:4573–4580. [PubMed: 25836494]

262. Shalaby M, Hauri CP. Demonstration of a low-frequency three-dimensional terahertz bullet with extreme brightness. Nat Commun. 2015; 6

263. Lu J, Zhang Y, Hwang HY, Ofori-Okai BK, Fleischer S, Nelson KA. Nonlinear two-dimensional terahertz photon echo and rotational spectroscopy in the gas phase. Proc Natl Acad Sci. 2016; 113:11800–11805. [PubMed: 27702903]

264. Savolainen J, Ahmed S, Hamm P. Two-dimensional raman-terahertz spectroscopy of water. Proc Natl Acad Sci. 2013; 110:20402–20407. [PubMed: 24297930]
265. Finneran IA, Welsch R, Allodi MA, Miller TF, Blake GA. Coherent two-dimensional terahertz-terahertz-raman spectroscopy. Proc Natl Acad Sci. 2016; 113:6857–6861. [PubMed: 27274067]
266. Woerner M, Kuehn W, Bowlan P, Reimann K, Elsaesser T. Ultrafast two-dimensional terahertz spectroscopy of elementary excitations in solids. New J Phys. 2013; 15:025039.
267. Xie X, Dai J, Zhang X-C. Coherent control of THz wave generation in ambient air. Phys Rev Lett. 2006; 96:075005. [PubMed: 16606102]
268. DAmico C, Houard A, Franco M, Prade B, Mysyrowicz A, Couairon A, Tikhonchuk V. Conical forward THz emission from femtosecond-laser-beam filamentation in air. Phys Rev Lett. 2007; 98:235002. [PubMed: 17677911]
269. Ho I-C, Guo X, Zhang X-C. Design and performance of reflective terahertz air-biased-coherent-detection for time-domain spectroscopy. Opt Express. 2010; 18:2872–2883. [PubMed: 20174116]
270. Karpowicz N, Lu X, Zhang X-C. Terahertz gas photonics. J Mod Opt. 2009; 56:1137–1150.
271. Thomson MD, Blank V, Roskos HG. Terahertz white-light pulses from an air plasma photo-induced by incommensurate two-color optical fields. Opt Express. 2010; 18:23173–23182. [PubMed: 21164658]
272. Andreeva V, Kosareva O, Panov N, Shipilo D, Solyankin P, Esaulkov M, de Alaiza Martínez PG, Shkurinov A, Makarov V, Bergé L, et al. Ultrabroad terahertz spectrum generation from an air-based filament plasma. Phys Rev Lett. 2016; 116:063902. [PubMed: 26918992]
273. Good JT, Holland DB, Finneran IA, Carroll PB, Kelley MJ, Blake GA. A decade-spanning high-resolution asynchronous optical sampling tera-hertz time-domain and frequency comb spectrometer. Rev Sci Instrum. 2015; 86:103107. [PubMed: 26520940]
274. Burghoff D, Kao T-Y, Han N, Chan CWI, Cai X, Yang Y, Hayton DJ, Gao J-R, Reno JL, Hu Q. Terahertz laser frequency combs. Nat Photon. 2014; 78:035107.
275. Rösch M, Scalari G, Villares G, Bosco L, Beck M, Faist J. On-chip, self-detected terahertz dual-comb source. Appl Phys Lett. 2016; 108:171104.
276. Rösch M, Scalari G, Beck M, Faist J. Octave-spanning semiconductor laser. Nat Photon. 2015; 9:42–47.
277. Tammaro S, Pirali O, Roy P, Lampin J-F, Ducournau G, Cuisset A, Hindle F, Mouret G. High density terahertz frequency comb produced by coherent synchrotron radiation. Nat Commun. 2015; 6
278. Rösch M, Scalari G, Beck M, Faist J. Octave-spanning semiconductor laser. Nat Photon. 2015; 9:42–47.
279. Barbieri S, Ravaro M, Gellie P, Santarelli G, Manquest C, Sirtori C, Khanna SP, Linfield EH, Davies AG. Coherent sampling of active mode-locked terahertz quantum cascade lasers and frequency synthesis. Nat Photon. 2011; 5:306–313.
280. Hsieh Y-D, Nakamura S, Abdelsalam DG, Minamikawa T, Mizutani Y, Yamamoto H, Iwata T, Hindle F, Yasui T. Dynamic terahertz spectroscopy of gas molecules mixed with unwanted aerosol under atmospheric pressure using fibre-based asynchronous-optical-sampling terahertz time-domain spectroscopy. Sci Rep. 2016; 6:28114. [PubMed: 27301319]
281. Bigourd D, Cuisset A, Hindle F, Matton S, Bocquet R, Mouret G, Cazier F, Dewaele D, Nouali H. Multiple component analysis of cigarette smoke using THz spectroscopy, comparison with standard chemical analytical methods. Appl Phys B. 2007; 86:579–586.
282. Jacobsen RH, Mittleman D, Nuss M. Chemical recognition of gases and gas mixtures with terahertz waves. Opt Lett. 1996; 21:2011–2013. [PubMed: 19881876]
283. Yardimci NT, Yang S-H, Berry CW, Jarrahi M. High-power terahertz generation using large-area plasmonic photoconductive emitters. IEEE Trans Terahertz Sci Technol. 2015; 5:223–229.
284. Shen Y, Lo T, Taday P, Cole B, Tribe W, Kemp M. Detection and identification of explosives using terahertz pulsed spectroscopic imaging. Appl Phys Lett. 2005; 86:241116.
285. Anastasi, RF., Madaras, EI., Seebo, JP., Smith, SW., Lomness, JK., Hintze, PE., Kammerer, CC., Winfree, WP., Russell, RW. Terahertz nde application for corrosion detection and evaluation under shuttle tiles. The 14th International Symposium on: Smart Structures and Materials &

Nondestructive Evaluation and Health Monitoring; International Society for Optics and Photonics; 2007. p. 65310W-65310W.

286. Gurney KR, Romero-Lankao P, Seto KC, Hutyra LR, Duren R, Kennedy C, Grimm NB, Ehleringer JR, Marcotullio P, Hughes S, Pincetl S, Chester MV, Runfola DM, Feddema JJ, Sperling J. Climate change: Track urban emissions on a human scale. Nature. 2015; 525:179–181. [PubMed: 26354467]
287. Petit JR, Jouzel J, Raynaud D, Barkov NI, Barnola J-M, Basile I, Bender M, Chappellaz J, Davis M, Delaygue G, Delmotte M, Kotlyakov VM, Legrand M, Lipenkov VY, Lorius C, PÉpin L, Ritz C, Saltzman E, Stievenard M. Climate and atmospheric history of the past 420,000 years from the Vostok ice core Antarctica. Nature. 1999; 399:429–436.
288. Elsig J, Schmitt J, Leuenberger D, Schneider R, Eyer M, Leuenberger M, Joos F, Fischer H, Stocker TF. Stable isotope constraints on Holocene carbon cycle changes from an Antarctic ice core. Nature. 2009; 461:507–510. [PubMed: 19779448]
289. Bock M, Schmitt J, Möller L, Spahni R, Blunier T, Fischer H. Hydrogen Isotopes Preclude Marine Hydrate CH_4 Emissions at the Onset of Dansgaard-Oeschger Events. Science. 2010; 328:1686–1689. [PubMed: 20576890]
290. Wolff EW, Chappellaz J, Blunier T, Rasmussen SO, Svensson A. Millennial-scale variability during the last glacial: The ice core record. Quaternary Science Reviews. 2010; 29:2828–2838.
291. Jimenez JL, Canagaratna MR, Donahue NM, Prevot ASH, Zhang Q, Kroll JH, DeCarlo PF, Allan JD, Coe H, Ng NL, Aiken AC, Docherty KS, Ulbrich IM, Grieshop AP, Robinson AL, Duplissy J, Smith JD, Wilson KR, Lanz VA, Hueglin C, Sun YL, Tian J, Laaksonen A, Raatikainen T, Rautiainen J, Vaattovaara P, Ehn M, Kulmala M, Tomlinson JM, Collins DR, Cubison MJE, Dunlea J, Huffman JA, Onasch TB, Alfarra MR, Williams PI, Bower K, Kondo Y, Schneider J, Drewnick F, Borrmann S, Weimer S, Demerjian K, Salcedo D, Cottrell L, Griffin R, Takami A, Miyoshi T, Hatakeyama S, Shimono A, Sun JY, Zhang YM, Dzepina K, Kimmel JR, Sueper D, Jayne JT, Herndon SC, Trimborn AM, Williams LR, Wood EC, Middlebrook AM, Kolb CE, Baltensperger U, Worsnop DR. Evolution of Organic Aerosols in the Atmosphere. Science. 2009; 326:1525–1529. [PubMed: 20007897]
292. Seinfeld, JH., Pandis, SN. Atmospheric Chemistry and Physics: From Air Pollution to Climate Change. Wiley; 2016.
293. Dockery DW, Pope CA. Acute respiratory effects of particulate air pollution. Annu Rev Public Health. 1994; 15:107–132. [PubMed: 8054077]
294. Pope CA, Dockery DW, Schwartz J. Review of Epidemiological Evidence of Health Effects of Particulate Air Pollution. Inhal Toxicol. 1995; 7:1–18.
295. Pope CA, Thun MJ, Namboodiri MM, Dockery DW, Evans JS, Speizer FE, Heath CW. Particulate air pollution as a predictor of mortality in a prospective study of U.S. adults. Am J Respir Crit Care Med. 1995; 151:669–674. [PubMed: 7881654]
296. Dominici F, Wang Y, Correia AW, Ezzati M, Pope CA, Dockery DW. Chemical Composition of Fine Particulate Matter and Life Expectancy: In 95 US Counties Between 2002 and 2007. Epidemiology. 2015; 26:556–564. [PubMed: 25906366]
297. van Eijck A, Opatz T, Taraborrelli D, Sander R, Hoffmann T. New tracer compounds for secondary organic aerosol formation from β-caryophyllene oxidation. Atmospheric Environment. 2013; 80:122–130.
298. Hu WW, Campuzano-Jost P, Palm BB, Day DA, Ortega AM, Hayes PL, Krechmer JE, Chen Q, Kuwata M, Liu YJ, de Sá SS, McKinney K, Martin ST, Hu M, Budisulistiorini SH, Riva M, Surratt JD, St Clair JM, Isaacman-Van Wertz G, Yee LD, Goldstein AH, Carbone S, Brito J, Artaxo P, de Gouw JA, Koss A, Wisthaler A, Mikoviny T, Karl T, Kaser L, Jud W, Hansel A, Docherty KS, Alexander ML, Robinson NH, Coe H, Allan JD, Canagaratna MR, Paulot F, Jimenez JL. Characterization of a real-time tracer for isoprene epoxydiols-derived secondary organic aerosol (IEPOX-SOA) from aerosol mass spectrometer measurements. Atmos Chem Phys. 2015; 15:11807–11833.
299. Fermann ME, Hartl I. Ultrafast Fiber Laser Technology. IEEE J Sel Top Quantum Electron. 2009; 15:191–206.
300. Fermann ME, Hartl I. Ultrafast fibre lasers. Nature Photon. 2013; 7:868–874.

301. Erny C, Moutzouris K, Biegert J, Kühlke D, Adler F, Leitenstorfer A, Keller U. Mid-infrared difference-frequency generation of ultrashort pulses tunable between 3.2 and 4.8 μm from a compact fiber source. Opt Lett. 2007; 32:1138–1140. [PubMed: 17410261]
302. Neely TW, Johnson TA, Diddams SA. High-power broadband laser source tunable from 3.0 μm to 4.4 μm based on a femtosecond Yb:fiber oscillator. Opt Lett. 2011; 36:4020–4022. [PubMed: 22002372]
303. Gambetta A, Ramponi R, Marangoni M. Mid-infrared optical combs from a compact amplified Er-doped fiber oscillator. Opt Lett. 2008; 33:2671–2673. [PubMed: 19015704]
304. Iwakuni K, Okubo S, Tadanaga O, Inaba H, Onae A, Hong F-L, Sasada H. Generation of a frequency comb spanning more than 3.6 octaves from ultraviolet to mid infrared. Opt Lett. 2016; 41:3980. [PubMed: 27607952]
305. Foster MA, Turner AC, Lipson M, Gaeta AL. Nonlinear optics in photonic nanowires. Opt Express. 2008; 16:1300. [PubMed: 18542203]
306. Lau RKW, Lamont MRE, Griffith AG, Okawachi Y, Lipson M, Gaeta AL. Octave-spanning mid-infrared supercontinuum generation in silicon nanowaveguides. Opt Lett. 2014; 39:4518–4521. [PubMed: 25078217]
307. Singh N, Hudson DD, Yu Y, Grillet C, Jackson SD, Casas-Bedoya A, Read A, Atanackovic P, Duval SG, Palomba S, Luther-Davies B, Madden S, Moss DJ, Eggleton BJ. Midinfrared supercontinuum generation from 2 to 6 μm in a silicon nanowire. Optica. 2015; 2:797.
308. Kuyken B, Ideguchi T, Holzner S, Yan M, Hänsch TW, Van Campenhout J, Verheyen P, Coen S, Leo F, Baets R, Roelkens G, Picqué N. An octave-spanning mid-infrared frequency comb generated in a silicon nanophotonic wire waveguide. Nat Commun. 2015; 6:6310. [PubMed: 25697764]
309. Johnson AR, Mayer AS, Klenner A, Luke K, Lamb ES, Lamont MRE, Joshi C, Okawachi Y, Wise FW, Lipson M, Keller U, Gaeta AL. Octave-spanning coherent supercontinuum generation in a silicon nitride waveguide. Opt Lett. 2015; 40:5117. [PubMed: 26512533]
310. Singh N, Hudson DD, Eggleton BJ. Silicon-on-sapphire pillar waveguides for Mid-IR supercontinuum generation. Opt Express. 2015; 23:17345. [PubMed: 26191744]
311. Del'Haye P, Herr T, Gavartin E, Gorodetsky ML, Holzwarth R, Kippenberg TJ. Octave Spanning Tunable Frequency Comb from a Microresonator. Phys Rev Lett. 2011; 107:063901. [PubMed: 21902324]
312. Kippenberg TJ, Holzwarth R, Diddams SA. Microresonator-Based Optical Frequency Combs. Science. 2011; 332:555–559. [PubMed: 21527707]
313. Jost JD, Lucas E, Herr T, Lecaplain C, Brasch V, Pfeiffer MHP, Kippenberg TJ. All Optical Stabilization of a Soliton Frequency Comb in a Crystalline Microresonator. Opt Lett. 2015; 40:4723. [PubMed: 26469604]
314. Yi X, Yang Q-F, Yang KY, Suh M-G, Vahala K. Soliton frequency comb at microwave rates in a high-Q silica microresonator. Optica. 2015; 2:1078.
315. Yu M, Okawachi Y, Griffith AG, Lipson M, Gaeta AL. Mode-locked mid-infrared frequency combs in a silicon microresonator. Optica. 2016; 3:854.
316. Suh M-G, Yang Q-F, Yang KY, Yi X, Vahala K. Microresonator Soliton Dual-Comb Spectroscopy. Science. 2016
317. Herr T, Brasch V, Jost JD, Wang CY, Kondratiev NM, Gorodetsky ML, Kippenberg TJ. Temporal solitons in optical microresonators. Nature Photon. 2014; 8:145–152.
318. Del'Haye P, Beha K, Papp SB, Diddams SA. Self-Injection Locking and Phase-Locked States in Microresonator-Based Optical Frequency Combs. Phys Rev Lett. 2014; 112:043905. [PubMed: 24580454]
319. Joshi C, Jang JK, Luke K, Ji X, Miller SA, Klenner A, Okawachi Y, Lipson M, Gaeta AL. Thermally controlled comb generation and soliton modelocking in microresonators. Opt Lett. 2016; 41:2565. [PubMed: 27244415]
320. Kourogi M, Nakagawa K, Ohtsu M. Widespan optical frequency comb generator for accurate optical frequency difference measurement. IEEE J Quantum Electron. 1993; 29:2693–2701.
321. Diddams SA, Ma L-S, Ye J, Hall JL. Broadband optical frequency comb generation with a phase-modulated parametric oscillator. Opt Lett. 1999; 24:1747. [PubMed: 18079922]

322. Long DA, Fleisher AJ, Douglass KO, Maxwell SE, Bielska K, Hodges JT, Plusquellic DF. Multiheterodyne spectroscopy with optical frequency combs generated from a continuous-wave laser. Opt Lett. 2014; 39:2688–2690. [PubMed: 24784078]
323. Martín-Mateos P, Jerez B, Acedo P. Dual electro-optic optical frequency combs for multiheterodyne molecular dispersion spectroscopy. Opt Express. 2015; 23:21149. [PubMed: 26367964]
324. Del'Haye P, Papp SB, Diddams SA. Hybrid Electro-Optically Modulated Microcombs. Phys Rev Lett. 2012; 109:263901. [PubMed: 23368562]
325. Hugi A, Villares G, Blaser S, Liu HC, Faist J. Mid-infrared frequency comb based on a quantum cascade laser. Nature. 2012; 492:229–233. [PubMed: 23235876]
326. Villares G, Hugi A, Blaser S, Faist J. Dual-comb spectroscopy based on quantum-cascade-laser frequency combs. Nat Commun. 2014; 5:5192. [PubMed: 25307936]
327. Villares G, Wolf J, Kazakov D, Süess MJ, Hugi A, Beck M, Faist J. On-chip dual-comb based on quantum cascade laser frequency combs. Appl Phys Lett. 2015; 107:251104.
328. Petruci, JFdS, Cardoso, AA., Wilk, A., Kokoric, V., Mizaikoff, B. iCONVERT: An Integrated Device for the UV-Assisted Determination of H_2S via Mid-Infrared Gas Sensors. Anal Chem. 2015; 87:9580–9583. [PubMed: 26369573]
329. Haas J, Mizaikoff B. Advances in Mid-Infrared Spectroscopy for Chemical Analysis. Annu Rev Anal Chem. 2016; 9:45–68.
330. Hunger D, Steinmetz T, Colombe Y, Deutsch C, Hänsch TW, Reichel J. A fiber Fabry–Perot cavity with high finesse. New J Phys. 2010; 12:065038.
331. Ott K, Garcia S, Kohlhaas R, Schüppert K, Rosenbusch P, Long R, Reichel J. Millimeter-long fiber Fabry-Perot cavities. Opt Express. 2016; 24:9839. [PubMed: 27137597]
332. Cole GD, Zhang W, Bjork BJ, Follman D, Heu P, Deutsch C, Sonderhouse L, Robinson J, Franz C, Alexandrovski A, Notcutt M, Heckl OH, Ye J, Aspelmeyer M. High-performance near- and midinfrared crystalline coatings. Optica. 2016; 3:647.
333. Baumgartner EW, Schwarzl T, Springholz G, Heiss W. Highly efficient epitaxial Bragg mirrors with broad omnidirectional reflectance bands in the midinfrared. Appl Phys Lett. 2006; 89:051110.
334. Schwarzl T, Eibelhuber M, Heiss W, Kaufmann E, Springholz G, Winter A, Pascher H. Mid-infrared high finesse microcavities and vertical-cavity lasers based on IV–VI semiconductor/BaF_2 broadband Bragg mirrors. J Appl Phys. 2007; 101:093102.
335. Koeninger A, Boehm G, Meyer R, Amann M-C. $BaCaF_2$/III–V semiconductor broadband distributed Bragg reflectors for long-wavelength VC-SEL and SESAM devices. Appl Phys B. 2014; 117:1091– 1097.
336. Lehmann KK, Johnston PS, Rabinowitz P. Brewster angle prism retroreflectors for cavity enhanced spectroscopy. Appl Opt. 2009; 48:2966–2978. [PubMed: 19488107]
337. Lee B, Lehmann K, Taylor J, Yalin A. A high-finesse broadband optical cavity using calcium fluoride prism retroreflectors. Opt Express. 2014; 22:11583. [PubMed: 24921279]
338. Hutzler NR, Lu H-I, Doyle JM. The Buffer Gas Beam: An Intense, Cold, and Slow Source for Atoms and Molecules. Chem Rev. 2012; 112:4803–4827. [PubMed: 22571401]
339. Spaun B, Changala PB, Patterson D, Bjork BJ, Heckl OH, Doyle JM, Ye J. Continuous probing of cold complex molecules with infrared frequency comb spectroscopy. Nature. 2016; 533:517–520. [PubMed: 27144351]
340. Grob, RL., Barry, EF. Modern Practice of Gas Chromatography. John Wiley & Sons; 2004.
341. McNair, HM., Miller, JM. Basic Gas Chromatography. John Wiley & Sons; 2011.
342. Qin Y, Gianchandani YB. A fully electronic microfabricated gas chromatograph with complementary capacitive detectors for indoor pollutants. Microsyst Nanoeng. 2016; 2:15049.

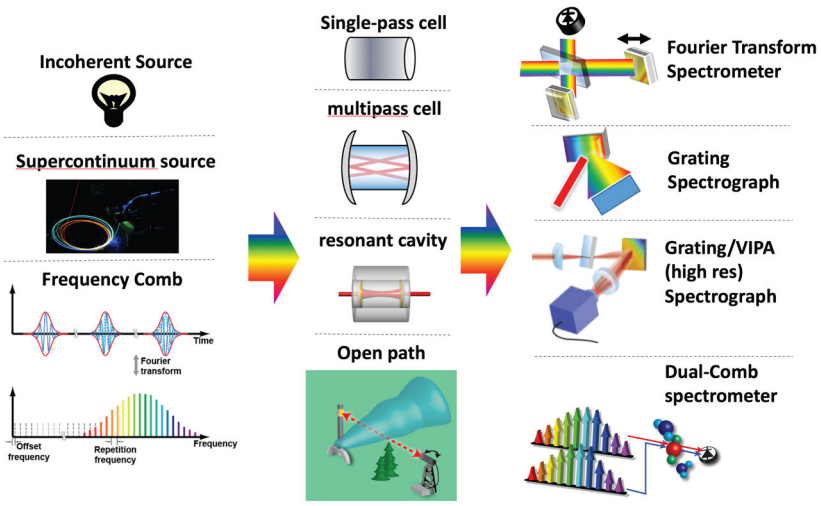

Fig. 1.

Overview of broadband spectroscopy systems. Left column: broad-band light sources. Middle column: absorption cells. Right column: broad-band detectors.

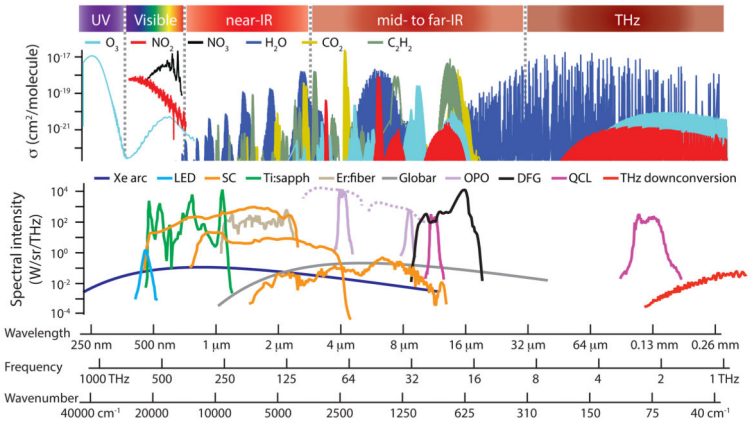

Fig. 2.

Example molecular cross sections and available sources in different spectral regions. For the laser based sources, we assume a 1 mrad divergence. For tunable sources, the tuning range is given by dashed lines. Cross-section data: [95] (NIR to THz), [148] (UV/Vis O_3), [149] (vis NO_2), [150] (vis NO_3). Spectral source data: Xe arc lamp (blackbody at 6000 K, $\varepsilon = 0.4$, 450 W total power), blue LED (5W blue LedEngin LZ1-00B205), visible supercontinuum (estimate), Ti:sapphire comb with nonlinear fiber ([151]), Er:fiber comb with nonlinear fiber ([152]), near-IR supercontinuum ([120]), mid-IR supercontinuum ([122]), globar thermal source (blackbody at 1000 K, $\varepsilon = 0.8$, 140 W total power), periodically-poled litium niobate (PPLN) optical parametric oscillator (OPO) frequency comb ([141]), gallium phosphide (GaP) OPO comb ([142]), difference-frequency generation (DFG) ([146]), QCL frequency comb (two different sources, [153]), THz downconversion ([154]).

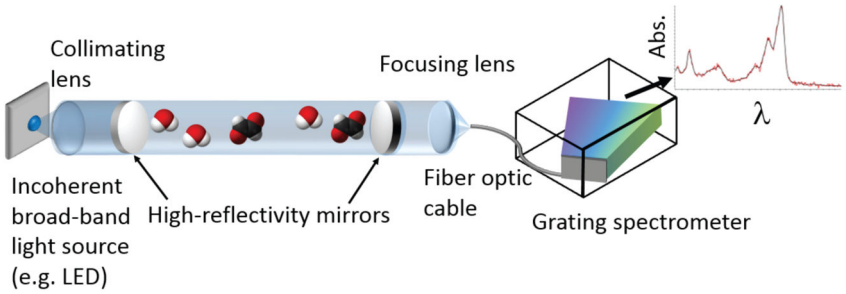

Fig. 3.

Example simplified schematic of IBB-CES and CE-DOAS setups. These consist of an incoherent light source, a collimating lens, a cavity made of a pair of highly reflective mirrors, a focusing lens after the cavity, and a fiber optic cable to transfer the light to the grating spectrometer. Data: example CE-DOAS glyoxal measurement (red: measured spectrum, black: fitted cross section).

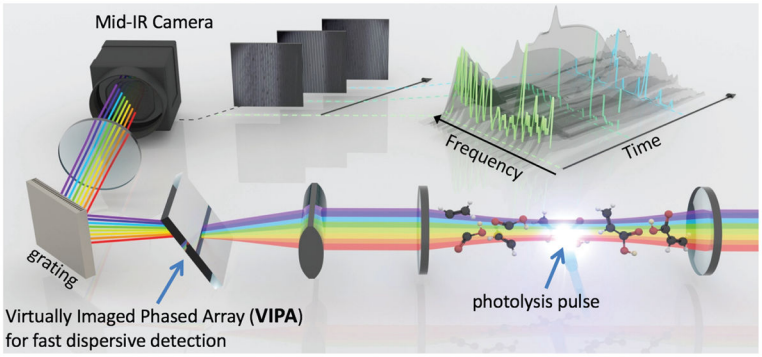

Fig. 4.

TRFCS. Laser light enters the cavity where a pulse starts the reaction through photolysis. Here, a VIPA spectrometer is used for detection. By measuring spectra at varying delays after the pulse, a complete kinetic picture can be determined (inset). Figure credit: The Ye Lab and Brad Baxley/JILA

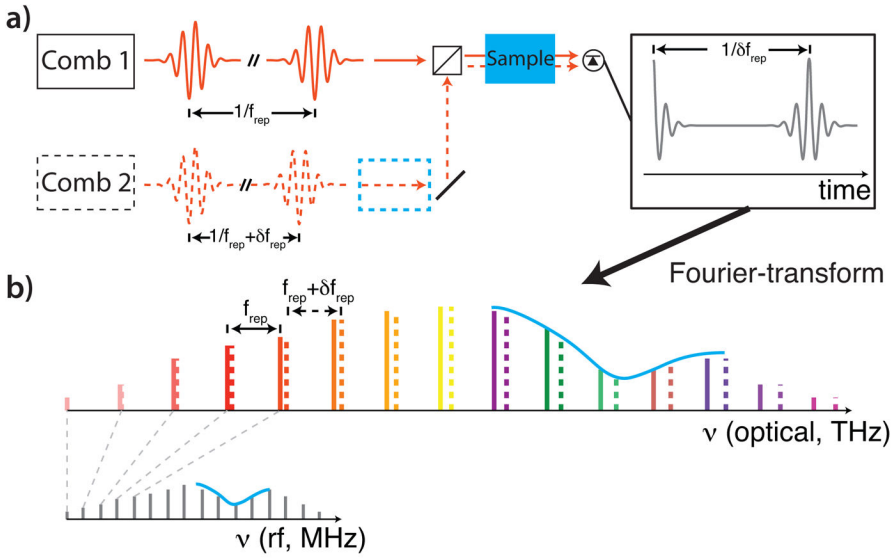

Fig. 5.

Dual comb spectroscopy, see text for details: (a) time-domain picture, (b) frequency-domain picture. The sample can be placed either before the combiner (dashed blue box) to measure both phase and absorbance or after the combiner (solid box) to measure only absorbance.

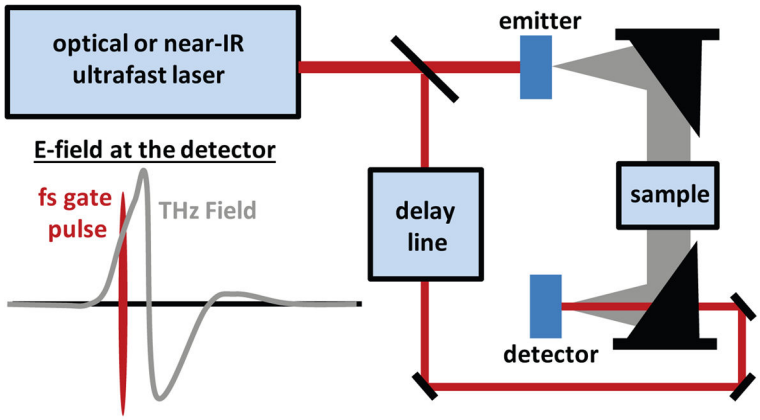

Fig. 6.

A generalized THz-TDS setup. The ultrafast pulses from an optical or near-IR laser are used to generate and detect THz transients. Detection is performed in the time domain with an optical delay line, and is sensitive to the THz electric field. This allows the measurement of the real and imaginary optical constants of a sample.

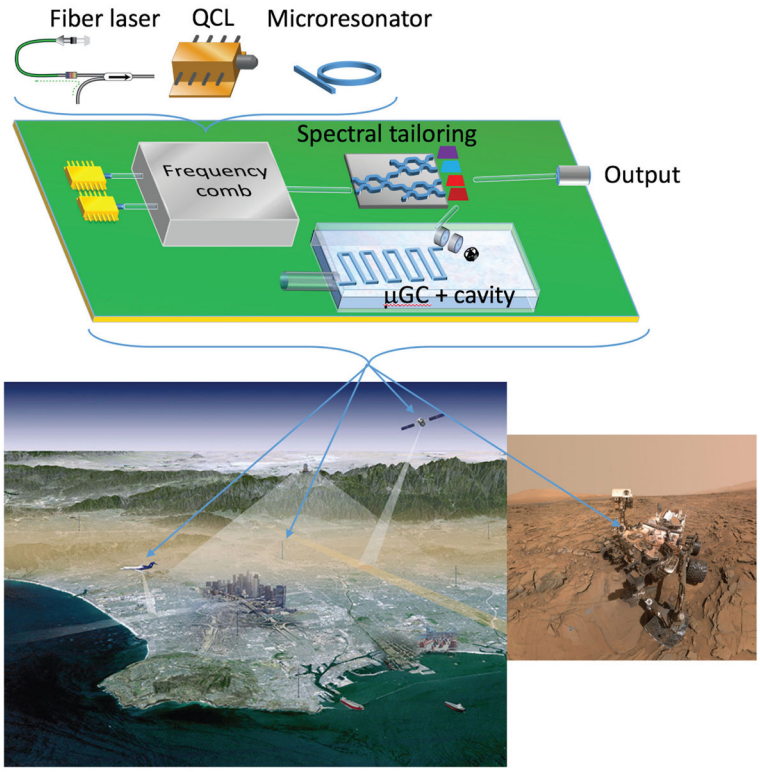

Fig. 7.

Outlook: A miniature broad-band light source (e.g., a fiber laser, mode-locked QCL, or mode-locked microresonator) is combined on-chip waveguides to produce light in targeted spectral bands for spectroscopy. A micro GC on a chip separates complex samples and sends molecules into a microcavity which allows for high sensitivity of the micro-comb (upper figure). Due to the small size and low power requirements, these instruments can be deployed on aircraft, satellites, or sensor networks in cities (lower left) or as instruments on rovers that visit other planets (lower right). Lower left and lower right figures courtesy of NASA/JPL-Caltech.

Table 1

List of acronyms for techniques discussed in this paper.

Acronym	Definition	Section
BB-CRDS	Broad-Band Cavity Ring Down Spectroscopy	3.D
CE-DOAS	Cavity-Enhanced Differential Optical Absorption Spectroscopy	3.B
CE-DFCS	Cavity-Enhanced Direct Frequency Comb Spectroscopy	3.E
DCS	Dual Frequency Comb Spectroscopy	3.F
DOAS	Differential Optical Absorption Spectroscopy	3.B, 3.C
FTIR	Fourier Transform Infrared Spectroscopy	3.A
FTS	Fourier Transform Spectroscopy	3.A
IBB-CES	Incoherent Broad Band Cavity-Enhanced Spectroscopy	3.B
LP-DOAS	Long-Path Differential Optical Absorption Spectroscopy	3.C
ML-CEAS	Mode-Locked Cavity Enhanced Absorption Spectroscopy	3.E
THz-TDS	Terahertz Time-Domain Spectroscopy	3.G
TRFCS	Time-Resolved Frequency Comb Spectroscopy	3.E

Table 2

Example trace species in the boundary layer (lowest part of the troposphere). Greenhouse gases are significant contributors to climate change. Biogenic species are emitted from plants while anthropogenic species are emitted from human activities, and these react in the atmosphere with e.g. OH and O_3 to form oxidation products. Halogen oxides are often found in the marine boundary layer from e.g. seaweed, and ozone-depleting species contribute to the Antarctic ozone hole. From [23–26].

Compound	Concentration
Greenhouse Gases	
CH_4	1.7 ppmv
N_2O	300 ppbv
SF_6	4 pptv
Biogenic Species	
Terpenes (e.g. α-pinene)	0.03–2 ppbv
Isoprene	0.6–2.5 ppbv
Anthropogenic Species	
Alkanes	1–300 ppbv
Alkenes/Alkynes	0.01–10 ppbv
Aromatics	0.01–3 ppbv
H_2S	0–800 pptv
NH_3	0.02–100 ppbv
Oxidation Products	
HCHO	0.1–60 ppbv
Acetone	0.2–9 ppbv
Glyoxal (CHOCHO)	0.01–1 ppbv
NO_2	0.01–2000 ppbv
NO_3	1–500 ppbv
N_2O_5	$<$15 ppbv
Nitric Acid	0.1–50 ppbv
SO_2	0.01–10 ppbv
CO	200 ppbv
Halogen Oxides	
BrO	0.1–10 pptv
IO	0.1–2 pptv
Ozone-Depleting Species	
$CFCl_3$	268 pptv
CF_2Cl_3	533 pptv
CH_3Cl	500 pptv
Other halocarbon species	10–100 pptv

Table 3

Typical range for the most common trace species in human breath. From [48, 52–55].

Compound	Concentration
Methane	1–100 ppmv
CO	1–5 ppmv
Acetone	0.3–2.5 ppmv
N_2O	0.3–1.6 ppmv
Ammonia	0.1–1 ppmv
Methanol	~500 ppbv
Isoprene	30–300 ppbv
NO	1–80 ppbv
2,3–Butanedione	1–200 ppbv
Ethane	2–20 ppbv
Other VOCs	0.1–40 ppbv

Table 4

List of databases useful for high-resolution broad-band spectroscopy.

Database	Wavelength Region	Data Type	Reference
HITRAN and HITEMP	UV to THz	Line parameters	[94, 95]
MPI UV/Vis Spectral Database	UV to near IR	Measured cross sections	[96]
NIST Quantitative Infrared	IR	Measured cross sections	[97]
PNNL Northwest Infrared Database	near IR to far IR	Measured cross sections	[98]
Cologne Database for Molecular Spectroscopy	far IR and THz	Line parameters	[99, 100]
JPL Molecular Spectroscopy Database	sub-millimeter to microwave	Line parameters	[101]
GEISA	UV to THz	Line parameters	[102]

Table 5

Comparison of system sensitivity (both incoherent and laser-based using a variety of detection methods). They are given in approximately chronological order. SC: Supercontinuum light source. FC: Frequency Comb. We have selected a high sensitivity example from each type of system (e.g. CE-DFCS + VIPA detection) to give a general idea for the sensitivity but these numbers will vary some for each system depending on the exact configuration.

Ref	System	Light Source	Absorption Cell	Detection system	$(N\sigma L)^{1s}_{min}\,(\mathrm{Hz}^{-1/2})$	Eff. Path (km)	Resolution (GHz)	Bandwidth/Center λ (nm)/(nm)
[167]	OP-FTIR	Thermal	Open Path	FTS	1.7×10^{-2}	~ 0.4	30	22000/13600
[168]	BB-CRDS	Dye Laser	High-finesse cavity	Grating + CCD	4.1×10^{-2}	30	140	20/660
[169]	LP-DOAS	Xe-arc	Open path	Grating + PDA	1.6×10^{-2}	4.4	620	45/440
[130]	IBB-CES	SC	High-finesse cavity	Grating + CCD	4.3×10^{-3}	19	70	30/670
[170]	CE-DFCS	FC	High-finesse cavity	VIPA	6.0×10^{-3}	14	0.8	25/1600
[171]	CE-DOAS	LED	High-finesse cavity	Grating + PDA	1.6×10^{-3}	13	810	50/460
[172]	CE-DFCS	FC	High-finesse cavity	FTS	7.2×10^{-4}	1.3	0.8	200/3760
[173]	CE-DFCS	FC	High-finesse cavity	Grating + CCD	8.6×10^{-5}	9.2	13.5	4/430
[174]	DCS	FC	Single-pass cell	Dual Comb	9.3×10^{-4}	7.5×10^{-4}	0.1	100/1562
[175]	NICE-OFCS	FC	High-finesse cavity	FTS	2.0×10^{-3}	0.66	2	30/1575
[176]	DCS	FC	Open Path	Dual Comb	3.4×10^{-2}	2	0.1	70/1635